Stability and Polaronic Motion of Self-Trapped Holes in Silver Halides

Insight through DFT plus U Calculations

Loftager, Simon; Garcia-Fernandez, P.; Aramburu, J. A.; Moreno, M.; García Lastra, Juan Maria

Published in:
Journal of Physical Chemistry C

Link to article, DOI:
10.1021/acs.jpcc.6b01710

Publication date:
2016

Document Version
Peer reviewed version

Stability and Polaronic Motion of Self-Trapped Holes in Silver Halides: Insight through DFT+U Calculations

S. Loftager[1], P. García-Fernández[2], J.A. Aramburu[2], M. Moreno[2], J. M. Garcia-Lastra[1]

[1]Department of Energy Conversion and Storage, Technical University of Denmark. Fysikvej 309, 2800 Kgs. Lyngby, Denmark

[2]Departamento de Ciencias de la Tierra y Física de la Materia Condensada, Universidad de Cantabria, Avenida de los Castros s/n, 39005 Santander, Spain

Abstract

Polarons and their associated transport properties are a field of great current interest both in chemistry and physics. In order to further our understanding of these quasi-particles, we have carried out first-principles calculations of self-trapped holes (STH) in the model compounds AgCl and AgBr, where extensive experimental information exists. Our calculations confirm that the STH solely stabilizes in AgCl but with a binding energy of only 165 meV, an order of magnitude smaller than that found for the V_k center in KCl. Key contributions to this stabilization energy come from the local relaxation along breathing (a_{1g}) and Jahn-Teller (e_g) modes in the $AgCl_6^{4-}$ unit. In order to study the transfer of the STH among silver sites we (i) use first-principles calculations to obtain the hopping barrier of the STH to first and second neighbors, involving eight distinct paths, using first-principles and (ii) construct a simple model, based on Slater-Koster parameters, that highlights the similarity of polaron transfer with magnetic superexchange. This allows one understanding why the movement of STH to second neighbors is highly enhanced with respect to closer ones. In agreement with experimental data and the model, the present calculations prove the existence of a dominant mechanism of polaronic motion that corresponds to the displacement of the STH to the next nearest sites in the <100> direction and a small barrier of 37 meV. This mechanism is dominated by the covalency inside a AgX_6^{4-} complex (X:Cl;Br) thus explaining why the STH is not stabilized in AgBr following the increase of covalency due to the Cl$\rightarrow$Br substitution. The present calculations confirm that ~10% of the charge associated with the STH in AgCl is lying outside the $AgCl_6^{4-}$ complex. This fact is behind the differences between optical and magnetic properties of the STH in AgCl and those observed in KCl:Ag^{2+}.

1. INTRODUCTION

The advent of quantum mechanics in 1926 played a fundamental role to understand the behavior of electrons in solids. Specifically, it allowed to rationalize the existence of insulating and metallic compounds and explained why electrons in metals have a much smaller specific heat than that of a classical Boltzmann gas. This insight was initially gained by assuming that valence electrons in crystals are well described by delocalized Bloch wave functions with nuclei that are essentially static and thus the electrons are characterized by an effective mass m*. Nevertheless, this understanding was quickly challenged as already in 1933 Landau suggested that a more stable situation could arise when an electron in a polarizable ionic lattice is localized to some extent following a simultaneous distortion of lattice ions[1]. This idea of a localized charge carrier composed by an electron (or hole) and its surrounding lattice distortion, called polaron, has had a strong influence in later research and it is nowadays often invoked to explain many atractive phenomena like high-temperature superconductivity in the cuprates[2-3] or colossal magnetoresistance in manganites[2, 4-5]. Furthermore, polarons play a key role in explaining transport in organic materials (both natural, like light-harvesting molecules in plants[6] or proteins key to the vision process in animals[7], and artificial[8], like organic light emitting diodes and transistors), or the performance of Li-air batteries where materials like Li_2O_2 and Li_2CO_3 are involved[9].

However, understanding in-detail the dynamics of these quasi-particles is far from trivial. From the very beginning most simple polaronic models refer to one of two kinds of limiting case[2]. On one hand, there are the so-called large or Fröhlich polarons[2, 10-11] where the electron is confined in a region much larger than the interatomic distance, typically 30 Å. In such a case the polaron behaves like a free electron but with a mass, m_p, higher than m* reflecting the electrostatic interaction between the electron and the distorted lattice which can be treated in the continuum approximation[2, 10-14]. A quite different situation holds for small or Holstein polarons[10, 14-15] favored by an increase of m*. In this case, at T = 0 K the electron is not free to move but it is self-trapped, although an increase of temperature favours its hopping to an equivalent position in the lattice. In this situation the electron is confined in a cavity whose size is of the order of the

lattice parameter and self-trapping is greatly influenced by the modification of bonding and interatomic distances involving the few ions residing in the cavity[12, 16].

Certification of the existence of a small polaron requires checking that the electron trapping is not due to any defect or unwanted impurity present in the crystal, a task which is not easy from the experimental side. First principle calculations can help to clear up this relevant issue if they actually prove that self-trapping is a spontaneous process. Nevertheless , this task is not simple as it requires the use of large supercells as well as an accurate treatment of electron correlation to account for the delicate balance of energies (particularly electron self-interaction) leading to localization of the charge carrier[7]. In systems of current technological interest, where intensive research is being carried out, this is further aggravated due to factors like structural disorder appearing in organic polymers[6] or magnetic disorder associated to the metal-insulator transition of the manganites[3].

The main goal of this work is to study in-depth the stability and dynamics of a small polaron formed in a *model* system using first-principles calculations. In this study particular attention is paid to explore the localization of the charge carrier and especially to quantify the different barriers which can, in principle, be involved in the hopping process. Moreover, we want to benchmark these techniques to simulate polarons against clear and well-contrasted experimental data.

Our chosen *model* systems are diamagnetic binary lattices with simple rocksalt structure, AgCl and AgBr, that have been extensively studied due to its relevance in photographic film technology[17-31]. As explained below, these experimental studies open important questions on the basic properties of polarons making them ideal to study the physics of these quasi-particles in detail.

Research on localized charge carriers in rocksalt-structure lattices started early after Landau[1] proposed his model for the self-trapped electrons. Although it was initially believed that F centers in alkali halides involve self-trapped electrons[32] no convincing evidence of a true self-trapping process was reported in the period 1933–1955. Despite this negative result, Mott and Gurney suggested that for alkali and silver halides, hole-trapping may take place more easily than

electron-trapping as the conduction band is wider than the valence band thus favoring the confinement[32].

The seminal work by Castner and Känzig using Electron Paramagnetic Resonance (EPR) strongly suggested that in X-ray-irradiated LiF, NaCl, KCl and KBr crystals at T = 77 K self-trapped holes (STHs) are actually formed giving rise to X_2^- radicals (X = halide), also called V_K centers[12, 33]. The lack of any defects in close proximity to V_K centers in alkali halides was later corroborated through Electron Nuclear Double Resonance (ENDOR) measurements which proved that a STH is *spontaneously* formed[34]. A first theoretical study showed that hole-trapping in KCl is mainly due to an energy gain of ~1.5 eV when the hole is captured by two adjacent X^- ions and its separation is then drastically reduced by ~30% to form the stable Cl_2^- species, involving six bonding but only five antibonding electrons[12, 16]. STHs in alkali halides become mobile above a certain temperature, equal to ~170 K for Cl_2^- in KCl[12]. In this process, that requires overcoming a barrier, the STH moves through the lattice *together with* a concomitant distortion, following the canonical definition of a mobile small polaron.

Concerning silver halides, EPR, ENDOR and cyclotron resonance data proved the formation of a STH in AgCl, but not in AgBr[17-19, 21, 23, 25-31, 35]. As a salient feature, the nature of the self-trapped species in the cubic AgCl crystal, formed after UV irradiation, is rather different from that found in alkali halides as the top of the valence band involves a strong admixture of 3p(Cl) and 4d(Ag) wave functions[29]. Indeed the resemblance of EPR data of KCl:Ag^{2+} or NaCl:Ag^{2+} [36-37] to those reported[19, 21, 23, 35] for the STH in AgCl (Table 1) proves that this species can be viewed, in a first approximation, as an *elongated* $AgCl_6^{4-}$ complex with the hole located in a x^2–y^2-type orbital resulting from a Jahn–Teller distortion. Despite this, the hyperfine and the isotropic superhyperfine constants measured for the STH in AgCl are somewhat smaller than those for KCl:Ag^{2+} or NaCl:Ag^{2+} [38](Table 1) thus suggesting that a fraction of the unpaired electron in AgCl is lying *outside* the $AgCl_6^{4-}$ complex.

The work by Laredo et al. demonstrated that STHs in AgCl become mobile above ~35 K[25]. Moreover, that study showed the existence of a *dominant* mechanism of polaronic hopping, involving an activation energy of 61 $\pm$ 3 meV[25], whose nature is hitherto unknown. As regards the

optical absorption transitions associated with the STH in AgCl, there is a band peaked at 1.2 eV measured experimentally whose origin has not been clarified yet[21, 27, 31]. Interestingly, when shinning the AgCl sample with this infrared light the concentration of STH decreases[21], a phenomenon that still needs to be understood.

After this review of available experimental data we see that there are several open questions of fundamental interest that we will try to respond in this work on small polarons in AgCl and AgBr: (i) What is the equilibrium geometry and the contribution of the local distortion to the binding energy of the STH in AgCl? (ii) What is the fraction of the unpaired electron outside the $AgCl_6^{4-}$ complex? (iii) Why is the STH stable in AgCl, but not in AgBr? (iv) What is the excitation responsible for the band peaked at 1.2 eV in AgCl? (v) By what mechanisms do the small polarons move through the AgCl lattice? It is worth noting that for answering the last but fundamental question there are already *eight* non-equivalent pathways in the *cubic* AgCl lattice which must be all scrutinized even if the study is restricted only to polaron hops to nearest or next-nearest silver ions.

This paper is structured in six sections. A simple model elucidating the origin of different barriers involved in the polaron motion along the AgCl lattice, including the influence of the Jahn–Teller effect , is presented in section 2. Section 3 covers the computational methods, paying special attention to the choice of the appropriate theoretical model required to describe AgCl and AgBr accurately. Sections 4 and 5 are focused on the stability and motion of polarons in AgCl while their optical properties are briefly discussed in section 6. Finally, the origin of the absence of a STH in AgBr is analyzed in some detail in section 7 and some final comments are provided in the last section.

2. ORIGIN OF THE HOPPING BARRIERS: SIMPLE MODELLING OF POLARON ENERGY SURFACES

While there exists a large bibliography on the theory of polarons[1, 10-11, 15, 39-40] we want to analyze here a simple model that provides an insight on: (a) the different properties of hole-doped AgCl and AgBr, and (b) the origin of the different hopping barriers for the localized polaron in AgCl. While the full treatment of polarons in AgCl requires necessarily the inclusion of the Jahn–Teller effect this hampers realizing a simple, analytical model providing an overview of the properties of

these systems. Thus, we will start providing such a model to improve it, in a second step, including more advanced features like the Jahn–Teller effect.

2.1. Non-degenerate two-site polaron model

We will start by considering a two-site model where both sites are completely equivalent and the electronic part can be described using a localized basis like, for example, the Wannier orbitals of a crystalline solid. We will call ψ_1 and ψ_2 to the basis functions localized at sites 1 and 2, respectively. In this first model (see Fig. 1) we will consider that the electrons localized in a particular site can interact with local distortions q_1 and q_2 that can be considered effective multimode interaction distortions[41-42]. Expanding the total Hamiltonian to second-order in these vibrations and considering that these local interactions do not interact among themselves we obtain

$$H\left(q_1,q_2\right)=H\left(q_1=0,q_2=0\right)+\frac{1}{2}\frac{\partial^2 H}{\partial q_1^2}q_1^2+\frac{1}{2}\frac{\partial^2 H}{\partial q_2^2}q_2^2+\frac{\partial H}{\partial q_1}q_1+\frac{\partial H}{\partial q_2}q_2 \tag{1}$$

Now, considering that the ground state of the system can be written as a Slater determinant, Ψ, where the orbitals can be expressed using the localized basis ψ_1 and ψ_2, we obtain the total energy as

$$E\left(q_1,q_2\right)=\frac{1}{2}K\left(q_1^2+q_2^2\right)+o^{-}\varepsilon^{-}+o^{+}\varepsilon^{+} \tag{2}$$

where $K = \langle \Psi |\partial^2 H/\partial q_i^2| \Psi \rangle$ is the local force constant for q_1 and q_2 and $o^{\pm}$ and $\varepsilon^{\pm}$ are, respectively, the occupations and energies of the low (-) and high (+) energy levels of the system (see Fig. 1) obtained from the diagonalization of the matrix

$$h=\begin{pmatrix}-\mathrm{v}\cdot q_1 & \gamma\\ \gamma & -\mathrm{v}\cdot q_2\end{pmatrix} \tag{3}$$

Here, $v = \langle \Psi_i |\partial H/\partial q_i| \Psi_i \rangle$ is the intra-site vibronic coupling and $\gamma = \langle \Psi_i |H(0,0)| \Psi_j \rangle < 0$ is the inter-site electronic hopping constant. This parameter, which is common in any tight binding

description, reflects the interactions between two equivalent close sites. Calculating the energy extrema of Eq. (2) with respect to q_1 and q_2 we can find the minima and the transition-states associated to the system. We find two kinds of solutions. The first one corresponds with the fully symmetric solution (Fig. 1) where $q_1 - q_2 = 0$ and the polaron is fully shared between both sites, i.e. the polaron is at the transition state between both sites. The second solution corresponds with the localization of the polaron in one single site and is characterized by two equivalent positions

$$q_1 - q_2 = \frac{\pm 2\sqrt{\left(o^+ - o^-\right)^2 \cdot E_{trap}^2 - \gamma^2}}{\mathrm{v}} \tag{4}$$

where $E_{trap} = -v^2/2K$ is the stabilization energy when one electron is fully localized in one site (self-trapping). The form of this stabilization energy is thus similar to that found for the linear vibronic coupling of a d^9 impurity in octahedral symmetry with both the symmetric a_{1g} and the e_g Jahn–Teller mode[7, 43]. A similar situation takes place for excited T states of Cr^{3+} and Mn^{2+} impurities under octahedral coordination[44-48].

We would like to note that while the transition state solution always exists, the localized one, characterized by Eq. (4), is *only* present when $\left|\left(o^+ - o^-\right)\cdot E_{trap}\right| > |\gamma|$. This inequality first implies that a localized solution will only exist if $o^+ \neq o^-$. Moreover, in such case a localized polaron can only be created when $|\gamma|$, which determines the band-width in a solid, is sufficiently small to be overcome by the distortion energy represented by E_{trap}. While the condition $o^+ \neq o^-$ is associated to interesting physics, like the magnetic state associated to double-exchange[49], in this work we will focus on the simplest case where there is only one electron or hole in the system, i.e. $o^+ - o^- = \pm 1$. It is worth noting that when $o^+ \neq o^-$ and $\left|\left(o^+ - o^-\right)\cdot E_{trap}\right| > |\gamma|$ holds the localized solution is always a minimum while the transition state solution can be a local maximum, i.e., a real transition state. Another interesting point is that the localized solutions are always minima while the transition state solution can be a local maximum (i.e., a real transition state) or a minimum (which would not be any more a transition state, but the ground state) depending on whether the localized solution exists (see Fig. 1). We can numerically characterize these situations with the energies of each kind of system configuration

$$E_{TS} = \frac{\left(o^{+} + o^{-}\right)^{2} E_{trap}}{2} + \left(o^{-} - o^{+}\right)\gamma \tag{5}$$

$$E_{loc} = \frac{\left(\left(o^{+} + o^{-}\right)^{2} + \left(o^{+} - o^{-}\right)^{2}\right) E_{trap}}{2} + \frac{\gamma^{2}}{2E_{trap}} \tag{6}$$

We see that in both Eqs. (5) and (6) there are two contributions to the stabilization, the first is proportional E_{trap} <0 and corresponds with lattice distortions while the second is associated to the inter-site interaction reflected in the γ parameter. We would like to note that the delocalized solution contains a self-trapping term as we are constraining the extra electron/hole to be localized in only two sites. If we had the infinite centers of the crystal this term would tend towards zero. Similarly, the localized solution, Eq.(6), contains a contribution coming from the inter-site interaction which is quadratic in γ and not linear such as it is found in Eq. (5). It is worth noting that the term in γ^2 in Eq (1.6) can be obtained assuming at zeroth-order perfect localization and applying second-order perturbation theory to obtain corrections due to the inter-site interaction (see Fig. 1). Using Eqs. (5) and (6) we can trivially find the barrier to polaron hopping as

$$B = E_{TS} - E_{loc} = \left(o^{-} - o^{+}\right)\gamma - \frac{\left(o^{-} - o^{+}\right)^{2} E_{trap}}{2} - \frac{\gamma^{2}}{2E_{trap}} \tag{7}$$

In Eq. (7) the last two terms are positive (E_{trap} is negative), and thus they contribute to make the barrier, *B*, larger. By contrast, the first one, depending linearly on $\gamma < 0$ is negative, thus acting to *reduce B*. From this simple model we can see that the main factor reducing the barrier for polaron hopping is the strength of the inter-site interaction described by the γ parameter. It is important to note that barrier, as expressed in Eq. (7), differs from that commonly used in polaronic model in that these only include the second term. This fact will be key to understand the different value of the barrier involved in the eight hopping processes explored in AgCl. At the same time it will be used to shed some light on the lack of a STH in AgBr as discussed on section 7.

2.2. Two-site Jahn-Teller polaron model

The previous model can be expanded to treat the more complicated case of STHs in silver halides. In this case we consider that the hole will localize around a silver center to form a AgX_6^{4-} (X = Cl^-, Br^-) complex which is thus somewhat similar to that found in X-irradiated alkali chlorides like NaCl or KCl initially doped with Ag^+ [36-37]. The conversion of Ag^+ into Ag^{2+} in AgCl due to hole trapping makes that the ground state of the octahedral $AgCl_6^{4-}$ complex is no longer an orbital singlet as the hole is placed in the highest occupied orbital of such center, which has e_g-symmetry. As a consequence, the ^2E_g ground state under octahedral symmetry becomes Jahn–Teller active (Fig. 2) and thus the final equilibrium geometry can be tetragonal due to the action of random strains present in any real crystal[50-51]. This very common situation is called static Jahn–Teller effect. In this case, the introduction of a hole involves two distortions, one associated to the symmetric a_{1g} breathing mode of the complex and another to the e_g Jahn–Teller mode involved in the distortion of the octahedral complex towards a tetragonal symmetry[43].

Bearing these facts in mind, if we firstly consider a *single* Ag^{2+} center in AgCl, using a linear vibronic coupling model there are two contributions to the self-trapping energy

$$E_{trap} = -\frac{v_{a_1}^2}{2K_{a_1}} - \frac{v_e^2}{2K_e} \qquad (8)$$

where v_{a_1}, v_e, K_{a_1} and K_e are, respectively, the linear vibronic coupling constants to a_{1g} and e_g local vibrational modes and their corresponding force constants. Comparison of Eq. (8) with the usual formulas for the Jahn–Teller effect reveals that the second term simply corresponds with the Jahn–Teller energy in the linear approximation, $E_{JT} = - v_e/2K_e$, while the first term corresponds to the stabilization energy of the a_{1g} breathing mode, termed E_{Br}.

Let us now consider a model with two equivalent silver centers among which, in the spirit of the model presented in section 2.1, the hole is going to move. In order not to overburden the model we are going to consider that all vibrational modes are local and that no interaction exists between them. Thus, each center has three available vibrational modes, the totally symmetric Q_{a_1} and the other two corresponding to the e_g Jahn–Teller mode, described by $Q_\theta \sim 3z^2 - r^2$ and $Q_\varepsilon \sim x^2 - y^2$ coordinates. Expanding the energy in a similar way to Eq. (1) but neglecting, so far, the inter-site

interaction, we can find that the localized solution has an energy equal to E_{trap} while the transition state has an energy equal to $E_{trap}/2$ making the barrier for the movement of the Jahn–Teller polaron in this localized limit,

$$B_{JT}^{loc} = \frac{-E_{trap}}{2} = \frac{-\left(E_{BR} + E_{JT}\right)}{2} \qquad (9)$$

As we learned from the model in section 2.1, this is simply an upper limit to the barrier, which will be *reduced*, when the inter-site interaction is included. If we now take into account the inter-site interaction by evaluating the term $H(q_i = 0)$ within the ground state we find an energy expression similar to Eq. (2) but involving four orbital energies (due to the two e_g orbitals involved) and 6 vibrations. The orbital energies are given by diagonalization of the following matrix

$$\begin{pmatrix} -\mathrm{v_e}Q_{\theta_1} - \mathrm{v_a}Q_{\mathrm{a}_1} & \mathrm{v_e}Q_{\varepsilon_1} & \gamma_{3z^2-r^2,3z^2-r^2} & \gamma_{3z^2-r^2,x^2-y^2} \\ \mathrm{v_e}Q_{\varepsilon_1} & \mathrm{v_e}Q_{\theta_1} - \mathrm{v_a}Q_{\mathrm{a}_1} & \gamma_{3z^2-r^2,x^2-y^2} & \gamma_{x^2-y^2,x^2-y^2} \\ \gamma_{3z^2-r^2,3z^2-r^2} & \gamma_{3z^2-r^2,x^2-y^2} & -\mathrm{v_e}Q_{\theta_2} - \mathrm{v_a}Q_{\mathrm{a}_2} & \mathrm{v_e}Q_{\varepsilon_2} \\ \gamma_{3z^2-r^2,x^2-y^2} & \gamma_{x^2-y^2,x^2-y^2} & \mathrm{v_e}Q_{\varepsilon_2} & \mathrm{v_e}Q_{\theta_2} - \mathrm{v_a}Q_{\mathrm{a}_2} \end{pmatrix} \qquad (10)$$

where, for instance, $\gamma_{x^2-y^2,x^2-y^2} = \left\langle x^2 - y^2 \middle| H(q_i = 0) \middle| x^2 - y^2 \right\rangle$ < 0 means an inter-site interaction between the x^2-y^2 orbitals of centers 1 and 2. All inter-sites interactions $\gamma_{i,j}$ (i, j = $3z^2$-r^2, x^2-y^2) can be expressed in terms of irreducible Slater-Koster parameters[52] as presented in Table 2.

It is worth noting now that the x^2-y^2 and $3z^2$-r^2 electronic levels are no longer degenerate as a result of a static Jahn–Teller effect. Indeed for $AgCl_6^{4-}$ complexes in alkali chlorides, as well as in AgCl, the elongated geometry with a hole in the x^2-y^2 orbital is energetically favorable with respect to a compressed one with the hole in $3z^2$-r^2 (Fig. 2) as demonstrated by EPR data[19, 21, 23, 36-37]. Along this line theoretical calculations carried out on KCl:Ag^{2+} and NaCl:Ag^{2+} reveal that the energy difference between compressed and elongated conformations is equal to 127 meV and 62 meV, respectively[53]. These relevant facts, whose actual origin is discussed in Refs.[43, 51, 53], support that in irradiated AgCl the hole is in a x^2-y^2-type orbital. Accordingly, as AgCl has the rocksalt structure the polaron motion should involve jumps from the hole in a x^2-y^2 orbital in the initial site to x^2-y^2, x^2-z^2 or y^2-z^2 orbitals belonging to close silver sites. In this work we consider the jumps to the 12 nearest

and also the 6 next-nearest silver ions in AgCl placed, respectively, at a distance R_S = 3.90 Å and R_S* = 5.51 Å. Although there are a total of 54 jumps some of them are however physically equivalent due to the cubic symmetry of the lattice. So, a jump from the initial site to a x^2-z^2 orbital of a nearest silver ion along the XZ axis is shortly described as XZ - x^2-z^2 and its corresponding inter-site interaction is written as $\gamma_{x^2-y^2;x^2-z^2}(XZ)$. This jump is physically equivalent to the YZ - y^2-z^2 jump. The eight physically non-equivalent jumps are detailed in Table 3 where equivalent jumps to a given one are reported as well.

The intersite matrix elements for such non-equivalent jumps can all be expressed in terms of Slater-Koster parameters[52] corresponding to nearest (V) and next nearest (V*) silver ions as shown on Table 4. As for transition metals the Slater-Koster parameters strongly decrease when the interatomic distance increases[13] it could be thought that the highest value of $|\gamma|$ and consequently the lowest value of the barrier would be reached for jumps to nearest ions. This statement is however not necessarily true for the present case as the intersite interactions $\gamma_{x^2-y^2;x^2-y^2}(Y)$ or $\gamma_{x^2-y^2;x^2-y^2}(XY)$ are greatly determined by the covalency at a single site and thus the overlap between the *ligand* wavefunctions involved in the two $|x^2\text{-}y^2\rangle$ *molecular orbitals*. For this reason the results shown in section 5 prove that the smallest barrier *B* for polaron motion in AgCl takes place for the Y - x^2-y^2 jump while it is clearly higher for the XY- x^2-y^2 jump.

Bearing these facts in mind and using Eqs. (8)-(10), the barrier for the Y - x^2-y^2 jump can be approximated by

$$B = B_{JT}^{loc} + \gamma_{x^2-y^2,x^2-y^2}(Y) \tag{11}$$

where B_{JT}^{loc}, defined in Eq. (9), is the barrier in the absence of any intersite interaction. For this reason, we expect that the difference between the largest and smallest barrier corresponding to the eight non-equivalent jumps should be close to $|\gamma_{x^2-y^2;x^2-y^2}(Y)|$.

3. COMPUTATIONAL METHODS

It is well-known that the Local-Density Approximation (LDA) and the Generalized-Gradient Approximation (GGA) functionals suffer from a coulombic self-interaction (SI) error, which tends to delocalized excess electrons and holes. Thus LDA and GGA are not appropriate for the purpose of the present work, i.e. to describe STHs in silver halides. There are various ways to overcome the SI error of the (semi)local DFT functionals. For instance, hybrids and orbital-dependent functionals stabilize electron localization, but they are computationally much more expensive than the LDA/GGAs. Modeling polaronic hopping requires large supercells and thus using hybrids or orbital-dependent functionals can become unaffordable. A computationally less demanding alternative to negate the SI error is to use Hubbard corrections, i.e. the DFT+U approximation. The DFT+ U method has been described in depth in the literature[54-56]. It has been extensively used in the study of transition-metal oxides where the U correction[57] is typically applied to the d orbitals of the transition metal[54-56, 58-60]. In other systems in which the localization of electrons or holes involves s and/or p orbitals, the U corrections are applied on these orbitals[9, 61-63].

In the particular case of AgCl, it has been experimentally shown that approximately 63% of the STH is localized in the p orbitals of the 6 Cl^- ions surrounding the Ag^{2+} ion[35]. On the other hand, numerous theoretical works have demonstrated the 5s(Ag) nature of the conduction band of AgCl and AgBr. Thus, it seems natural to apply the U corrections on the *np* orbitals of the halide ions (n = 3 for Cl and n = 4 for Br) and on the 5s(Ag) orbitals.

In order to determine the optimal value of the U corrections it is usual to track different values of U and use the ones that match a particular experimental parameter of the material, normally its band gap. In the particular case of AgCl and AgBr, we chose to map the dependence of both the direct ($\Gamma \rightarrow \Gamma$) and indirect ($L \rightarrow \Gamma$) band gaps upon the U correction on the *p* levels of the halide ions, $U_{\mathrm{Cl(p)}}$ and $U_{\mathrm{Br(p)}}$ for AgCl and AgBr, respectively, and upon the U correction on the 5s(Ag) levels, $U_{Ag(s)}$. We map the band-gap dependence upon the U correction using 0.25 eV intervals for U. As a basis for applying the U corrections we used the Wu–Cohen[64] (WC) and the PBEsol[65] GGA exchange–correlation functionals since both of them have shown very good agreement with experimental lattice parameters and elastic properties in other solids[66]. These calculations, performed to determine the optimal U corrections and exchange–correlation functional to describe pristine AgCl and AgBr materials, were performed with the real-space

projector-augmented-wave code, GPAW[67], with the structures set up in the Atomic Simulation Environment (ASE)[68]. The calculations were performed for the primitive cell shown in Fig. 2(a), using a grid spacing of 0.16 Å for the wave functions with a $8 \times 8 \times 8$ k-grid. No smearing was applied for the occupation of the electronic states.

Table **5** shows the optimal U corrections that match the direct and indirect band gaps of AgCl and AgBr, using WC and PBEsol functionals. Interestingly, the optimal U corrections are the same for WC and PBEsol functionals ($U_{\mathrm{Ag(s)}} = 4.0\,\mathrm{eV}$ and $U_{\mathrm{Cl(p)}} = 5.0\,\mathrm{eV}$ for AgCl, $U_{\mathrm{Ag(s)}} = 5.25\,\mathrm{eV}$ and $U_{\mathrm{Br(p)}} = 3.0\,\mathrm{eV}$ for AgBr) and that the calculated lattice parameters and bulk moduli are also very similar with both functionals such as it is shown on Table 5. Fig. 3 shows the calculated band structure using the optimal U corrections and the dependence of the direct and indirect band upon the U values (it is only shown for PBEsol+U; similar features were found using WC+U). It can be seen how the U correction on silver *s* orbitals (Figs. 3c and 3d) hardly affects the direct band gap of the materials, while it has a strong effect on their indirect band gap. On the other hand, the U correction on the *p* orbitals of the halide ions affects both the direct and indirect band gaps, being the effect slightly more pronounced in the latter. These differences in the dependence of the direct and indirect band gaps upon using either $U_{\mathrm{Ag(s)}}$ or $U_{\mathrm{Cl(p)/Br(p)}}$ corrections allowed us to match the direct and the indirect band gaps independently. Obviously, by construction, our PBEsol+U and WC+U band gaps are very close to the experimental ones (less than 2% error), not only improving significantly upon conventional GGA results reported in the literature (e.g. PBE[69] calculations by Wilson et al.[70] or Perdew–Wang[71] calculations by Benmessabih et al.[72]), but also upon hybrid (B3LYP[73] calculations by Rathor et al.[74]) and SI-corrected calculations (LDA-SIC calculations by Vogel[75] et al.). Additionally, the present calculated PBEsol+U and WC+U lattice parameters and bulk moduli displayed in Table 5 show a better agreement with the experimental figures than the aforementioned PBE, PW or LDA-SIC calculations.

Since the performance of WC+U and PBEsol+U functionals describing AgCl and AgBr properties is so similar, we had to make an arbitrary decision for the exchange–correlation functional for the study of STH localization and mobility in these materials. We chose to continue with the PBEsol+U functional for the calculations of the energy barriers associated the polaron

hops which were determined using the nudged-elastic-band (NEB) method where the minimum-energy paths were calculated[76]. Due to the size of the supercell, generated by a $3 \times 3 \times 3$ repetition of a cubic unit cell (using the optimized PBEsol lattice parameters in Table 1), used in the NEB calculations, it was sufficient only to consider the Γ point. A grid spacing of $h = 0.2$ Å was used. Electronic states were smeared to a width of 0.05 eV using a Fermi–Dirac distribution for the level occupations. All atoms were let to relax until the Hellmann–Feynman forces were below 0.06 eV/Å. The formation of hole polaron was studied by adding one hole to the supercell, keeping its neutrality by adding a uniform negative compensation charge. It should be remarked that when the perfect silver halide structures containing a positive excess charge of unity was relaxed, no localization of the hole was observed (i.e, the hole was completely delocalized). This delocalization occurring when the perfect structure of the host lattice is used as initial guess has been observed in other computational studies of polarons. Thus, the standard procedure is to break the host symmetry manually and then to carry out a relaxation of the geometry.[9, 77-78] In the present study, in order to localize the hole on a particular Ag ion it was necessary to prepare the system in a favorable initial configuration. We did this through the following procedure: We considered a $3 \times 3 \times 3$ NaCl supercell (imposing the AgCl lattice parameter calculated in table 5) with only one Ag atom replacing one Na atom (we chose NaCl due to its close experimental lattice parameter to AgCl). Under these conditions the hole gets localized straightforward on the silver ion, which becomes a Ag^{2+}ion. Subsequently, the rest of Na atoms in the supercell were substituted by Ag atoms, recovering the original AgCl system, but now with a geometry that favours localization of the hole on one single Ag^{2+} ion. Finally, this new geometry is used as starting point to relax the localized hole in the silver halide.

Finally and, in order to calculate the one-electron DFT Hamiltonian associated to the valence band of AgCl and AgBr in a localized basis we made use of Wannier90 code[79] as interfaced with VASP[80] using the HSE06 hybrid functional[81].

4. STABILITY OF SELF-TRAPPED HOLES IN AGCL

Both the compressed and the elongated hole-trapping structures of AgCl have been investigated. Let us first consider the localized B_{1g} state in AgCl involving an elongated geometry

characterized by two axial Cl^- ligands at a distance $R_0 + 2\varepsilon$ and four equatorial Cl^- ligands at a distance $R_0 - \varepsilon$ (Fig. 2c). At equilibrium, this localized situation was found to be *only* 165 meV more stable than the completely delocalized state thus implying a binding energy E_b=-0.165eV . Moreover, the localized B_{1g} state was found to be more stable by 56 meV than the A_{1g} state involving a compressed state, characterized by two axial Cl^- ligands at a distance $R_0 - 2\varepsilon$ and four equatorial Cl^- ligands at a distance $R_0 + \varepsilon$ (Fig. 2c). These results thus support that STHs can be *spontaneously* produced in irradiated AgCl. Moreover, they are consistent with experimental EPR and ENDOR data on this compound proving the formation of elongated $AgCl_6^{4-}$ complexes with the hole placed in the antibonding x^2-y^2 orbital[19, 23, 25, 27, 35].

Upon hole localization, the Ag^{2+}–Cl^- R_0 distance is found to be reduced by about 0.13 Å with respect to the Ag^+-Cl^- bond length in pristine AgCl material, R_L= 2.76 Å (Table 6). We observed that the R_0 values for elongation and compression are similar, whereas the ε value for elongation (ε = 0.119 Å) is about twice that of compression. It is worth noting that this situation is rather similar to that found for NaCl: $Ag^{2+}$where EPR data demonstrate that the unpaired electron is placed in the x^2-y^2 orbital and thus the $AgCl_6^{4-}$ complex is elongated[37]. Moreover, calculations carried out through a CASPT2 cluster model[53] for NaCl:Ag^{2+} lead to R_0 = 2.63 Å and ε = 0.09 Å and an energy difference between compressed and elongated conformations at equilibrium equal to 62 meV. These values are thus close to those obtained for the STH in AgCl, a situation which is helped by the similarity of metal-ligand distances in the perfect lattice, R_L, for AgCl (R_L = 2.76 Å) and NaCl (R_L = 2.82 Å). Interestingly, in the work by Trueba et al.[53] the so-called Jahn–Teller energy, $E_{JT,}$ has also been calculated. This stabilization energy is just the energy difference between the octahedral and tetragonal conformations at equilibrium and is found to be E_{JT} = 201 meV for NaCl: Ag^{2+} [53].

In order to calculate how much the local distortion around the Ag^{2+} ion stabilizes the localization of the hole (E_{trap} defined in Eq. (8)) in AgCl we need to sum the contributions from the Jahn–Teller distortion (E_{JT} in our model from section 2) and from the a_{1g} breathing vibrational mode (E_{BR} in our model from section 2). Nevertheless, it is not possible to compute E_{JT} in AgCl since the hole delocalizes if an octahedral symmetry is imposed to the $AgCl_6^{4-}$ complex. Thus taking into account the similarities between the STH in AgCl and NaCl: Ag^{2+} we have assumed a value E_{JT} =

201 meV for the former system. In order to estimate E_{BR} we have performed a calculation imposing distance $R_0 = R_L$ and keeping the Jahn–Teller distortion. From it we have obtained that the a_{1g} mode contributes with E_{BR} = 271 meV to stabilize the self-trapping of the hole, a quantity that is thus a bit higher than E_{JT} = 201 meV. It is worth noting that a similar situation to this one, where $E_{BR} \geq E_{JT}$, has been found exploring the first excited state of MnF_6^{4-} and $CrCl_6^{3-}$ complexes also involving a Jahn–Teller coupling with the e_g mode[45-46]. Nevertheless, in these systems E_{BR} and E_{JT} are both lying in the 30-60 meV range[45-46] and thus they are significantly smaller than in the present case consistently with a much smaller lattice relaxation. Along this line values of E_{JT} in the range 60-85 meV are also found for the ground sate of Cu^{2+} and Ag^{2+} in a *stiff* lattice like MgO[43]. These values, certainly smaller than that found for the present case, are helped by a bulk modulus of MgO (B = 160 GPa) which is about three times higher than that for AgCl and thus avoids bigger lattice relaxations. Thus, taking into account the values E_{JT} = 201 meV and E_{BR} = 271 meV, derived for $AgCl_6^{4-}$, in AgCl we obtain E_{trap} = 472 meV and B_{JT}^{loc} = 236 meV using Eqs. (8) and (9).

Let us now focus on a relevant issue, the amount of hole charge residing on silver and chlorine ligands as well as *outside* the $AgCl_6^{4-}$ complex in AgCl. For clearing up this issue we have calculated the local magnetic moment projected onto the ions (Table 7) of the distorted octahedron as it gives a good indication of the distribution of the hole on each ion. From the calculated distribution of the local magnetic moments of the elongated state, it was seen that the hole distributed itself 17% on the Ag^{2+} ion and 19% on each xy-plane Cl ligand in the same $AgCl_6^{4-}$ complex (Fig. 2b). These results are in very good agreement with the EPR/ENDOR determined hole distribution by Bennebroek et al.[19, 35], who measured approximately 19% STH on Ag^{2+} and 16% on *each* equatorial Cl^- ion. These figures thus imply that the hole is mostly residing on four equatorial ligands rather than on central Ag^{2+} ion a situation certainly unusual for octahedral ML_6 complexes (M = 3d cation; L = F, Cl). Nevertheless, an analysis of EPR data of KCl:Ag^{2+} [82] as well as Xα calculations on $AgCl_6^{4-}$ [83] already showed that only about 40% of the unpaired electron is on silver, a fact ultimately due to the high optical electronegativity of Ag^{2+} [82-83] when compared to that of 3d cations like Cu^{2+} or Ni^{2+} [84]. Interestingly, the DFT study in the present work also showed that X and Y Ag ions (Fig. 2b) had non-zero magnetic moment of $0.013\ \mu_B$, which is again in excellent agreement with experimental values of a d-orbital contribution to the spin density per nucleus of $0.014\ \mu_B$.[19, 35] This fact thus stresses the existence of unpaired electron charge lying

beyond the domain associated with the $AgCl_6^{4-}$complex. A detailed analysis of the present calculations leads to a total electronic charge of ~ 8% lying outside the complex region. This figure can be compared with the value (~15%) estimated from the analysis of ENDOR data[19, 35]. Along this line the present results on AgCl also point out that the fraction of electronic charge on silver would be smaller than for $AgCl_6^{4-}$ formed in $KCl:Ag^{2+}$. This conclusion is qualitatively consistent with the observed reduction of the two components of the hyperfine tensor on passing from $NaCl:Ag^{2+}$ or $KCl:Ag^{2+}$ to $AgCl_6^{4-}$ in AgCl (Table 1).

The analysis of the experimental superhyperfine tensor also provides with some hints on this issue. If the unpaired electron of a D_{4h} $AgCl_6^{4-}$complex resides in the antibonding b_{1g} level the associated wavefunction can shortly be written as

$$\left|b_{1g}\right\rangle = \alpha\left|x^2 - y^2\right\rangle - \beta_{p\sigma}\left|\chi_{p\sigma}\right\rangle - \beta_s\left|\chi_s\right\rangle \qquad (12)$$

Here $|\chi_{p\sigma}\rangle$ and $|\chi_s\rangle$ mean suitable linear combination of *np* and *ns* orbitals of ligands, where n = 3 for chlorine. Due to the big separation between 3p and 3s orbitals of free chlorine ion (15.9 eV) it has been shown that β_s^2 is essentially given by[85]

$$\beta_s^{\,2} \approx C\alpha^2 S_s^{\,2} \quad ; \quad S_s = \left\langle x^2 - y^2 \middle| \chi_s \right\rangle \qquad (13)$$

where C is a constant characteristic of the complex. Thus, if α^2 has the same value in AgCl, $NaCl:Ag^2$ or $KCl:Ag^{2+}$, β_s^2 is determined by the overlap integral S_s which increases significantly when the equatorial Ag^{2+}-Cl^- distance, R_{eq}, is reduced. By this reason, as R_{eq} is smaller for the STH in AgCl than for $NaCl:Ag^2$ or $KCl:Ag^{2+}$ (Table 1) one would expect that β_s^2 is higher for the former system *provided* α^2 is the same. As the isotropic superhyperfine constant A_s is essentially proportional to β_s^2 we see in Table 1 that A_s is however higher for $NaCl:Ag^2$ or $KCl:Ag^{2+}$ than for the STH in AgCl. This fact is again consistent, albeit qualitatively, with the reduction of α^2 on passing from $KCl:Ag^{2+}$ ($\alpha^2 \cong 40\%$) to the STH in AgCl ($\alpha^2 \cong 20\%$). On the other hand, as the anisotropic superhyperfine constant, A_p, reflects the dominant covalency with equatorial 3p chlorine ions, β_p^2, experimental data in Table 1 suggest rather similar values of β_p^2 for the STH in AgCl and Ag^{2+}-doped NaCl or KCl.

It is now worthwhile to compare the present results on the STH in AgCl with the local relaxation and binding energy, E_b , reached for the Cl_2^- center in KCl[12, 16]. In the last case (Table 8) if the two chlorine ions are initially separated in the perfect KCl lattice by R_L = 4.45 Å the final distance once the hole is trapped is strongly reduced to R = 2.96 Å implying $R_L - R$ = 1.49 Å[16]. The local relaxation for the STH in AgCl is however much smaller as $R_L - R_{ax}$ = -0.09 Å and $R_L - R_{eq}$ = 0.27 Å. Concerning the binding energy, E_b , aside from the energy involved in this relaxation or trapping process, $E_{trap}<0$, it also depends on the localization, $E_{Loc,}>0$ and polarization, $E_{pol}<0$ energies[12, 16]. $E_{Loc,}$ reflects the energy required to convert a free hole into a localized one which is roughly equal to half the extension of the valence band. E_{pol} is the energy gain due to the polarization, by a charge trapped into a cavity of radius R_C , of all ions residing outside. Interestingly the estimations carried out for the Cl_2^- center in KCl lead to $E_{Loc,} + E_{pol} \approx 0$[12, 16] thus implying that the binding energy, E_b= -1.5eV ,is close to E_{trap} which in turn reflects the local lattice relaxation (Table 8). A similar situation to this one takes place for the STH in AgCl although the value E_b= -0.165 eV derived from the present calculations is *one order of magnitude* smaller than the figure reported for the Cl_2^- center in KCl[12, 16]. This reduction thus mainly follows the corresponding decrease of E_{trap} which is consistent with the much lower local relaxation involved in the STH in AgCl than in Cl_2^- . The value $|E_b|$= 0.165eV , somewhat smaller than $|E_{trap}|$= 0.47 eV, underlines the difficulties for obtaining in the calculations a stable STH in AgCl.

5. POLARONIC HOPPING MECHANISMS IN AGCL

In order to find the dominant mechanism of polaronic motion in AgCl it is crucial to determine the barriers associated with the eight non-equivalent hops discussed in section 2 involving jumps to nearest and next-nearest neighbor silver ions. Accordingly, there are two kinds of hops that can be distinguished by their length in the perfect AgCl lattice, namely, short hops of R_S = 3.88 Å along the diagonals of the crystal (XY, XZ and YZ, shown in Fig. 4(a-d); see also Fig. 2b), and long hops of R_S^* = 5.49 Å along the crystallographic axes (X, Y and Z, shown in Fig. 4(e-h); see also Fig. 2b). As it has been pointed out in section 2 there is a second degree of freedom for the hops, that corresponds to the *orientation* of the STH in the destination Ag^{2+} ion (x^2-y^2, x^2-z^2, or y^2-z^2) with respect to the origin Ag^{2+} ion (where by convention we set the STH in the x^2-y^2 orientation). This gives rise to 54 different possible STH hops. However and, as already indicated,

only 8 out of these 54 hops are inequivalent by symmetry (see Table 3 to see the equivalent hop families).

If the hole jumps from a Ag^{2+} ion to a close Ag^{+} we can define an orthogonal coordinate system (ξ, η ,ζ) for the minimum energy path followed by the system so the hole is initially placed at (0, 0, 0) while the second site is at (ξ_1, 0, 0). The position (ξ_B, 0, 0), where $0 < \xi_B < \xi_1$, describes the maximum along the path i.e. the position of the barrier. If we calculate the total energy E(ξ) varying only the ξ coordinate we can obtain for every value of ξ the equilibrium geometry and the corresponding total energy using the NEB method[76]. From this study the barrier at T = 0 K for the eight non-equivalent hops can be calculated. The results of the present calculations for such non-equivalent hops in AgCl are gathered in Fig. 4 and also in Table 4 and fall into three classes: (i) Five hops with relatively high barriers of 179-198 meV shown in Fig. 4(a,c,d,f,g). (ii) A XY - x^2-y^2 hop with moderate barrier of 92 meV shown in Fig. 4(b). (iii) The Y - x^2-y^2 and X - x^2-z^2 hops, shown in Fig. 4(e,h), with a practically identical energy barrier (37 meV) which is the lowest one among all considered hops. All barrier profiles show very symmetric polaron hops. It is instructive to notice that the hops with high barriers (179-198 meV) require energies *slightly above* the energy of the delocalized state (165 meV). This implies that this type of hops will never occur as that would destroy the localized polaron. By contrast, looking at the Y - x^2-y^2 and X - x^2-z^2 hops, with a nearly identical energy barrier of only 37 meV, it is clear that the STH in AgCl is able to move along the three principal axes of the cube without destroying the polaron.

The results embodied in Fig. 4 can be analyzed taking into account the expression of the intersite matrix element, γ, collected in Table 4. According to the discussion in section 2, a decrease of $|\gamma|$ favours the increase of the barrier. If we first compare the hops to nearest silver ions (R_S = 3.90 Å) we see that the barrier (92 meV) for the XY - x^2-y^2 hop ($\gamma = -V_{dd\pi}$) is clearly smaller than that for the XZ - x^2-z^2 hop ($\gamma = -V_{dd\pi}/2$) involving a barrier of 179 meV. In the same vein, as $V_{dd\pi} > 0$ the expressions of Table 4 allow one to understand why the barrier for the XZ - y^2-z^2 hop (185 meV) is a bit smaller than that for the XZ - x^2-y^2 (198 meV). Moreover, if we keep the distance between close sites it is known[13] that $|V_{dd\sigma}| > V_{dd\pi} >> |V_{dd\delta}|$. For this reason, XZ - x^2-y^2 and

XZ - y^2-z^2 hops, whose inter-site matrix element is clearly dominated by $V_{dd\delta}$, have the highest value of the barrier among the four different hops to a nearest site.

Let us now focus on the results for the four inequivalent long hops (R_S^* = 5.51 Å) given in Fig. 4 and Table 4. As a salient feature the lowest energy barriers among the eight non-equivalent hops are found for the Y - x^2-y^2 and X - x^2-z^2 hops involving not a nearest but a next nearest neighbor. The energy barrier for such hops is practically identical to 37 meV, which is thus nearly 2.5 times smaller than the smallest barrier obtained for short hops. The nearly identical value for the energy barrier of Y - x^2-y^2 and X - x^2-z^2 hops is consistent with inter-site matrix elements dominated by $|V_{dd\sigma}^*| >> |V_{dd\delta}^*|$ (Table 4). By this reason, the Z - x^2-y^2 and Z - x^2-z^2 hops, depending only on $V_{dd\delta}^*$, exhibit a barrier which is about 5 times higher than that for Y - x^2-y^2 and X - x^2-z^2 hops.

The results embodied in Figure 4 and Table 4 shed light on the experimental work by Laredo et al.[25] proving the existence of a *dominant* mechanism of polaronic hopping above ~35 K, whose activation energy is 61 $\pm$ 3 meV. According to the present results such a *dominant* mechanism can be ascribed to Y - x^2-y^2 and X - x^2-z^2 hops though the present calculations slightly underestimate the value of the energy barrier. It is worth noting however that we have calculated *B* considering only the adiabatic limit, i.e. using transition state theory. This provides the lower bound of the barrier. However, as described by Marcus theory, when the non-adiabatic effects and the re-organization energy from the environment in a charge-transfer reaction are considered, *B* is in general larger than this lower bound[86]. Although this digression can help to understand the underestimation of *B* using using transition state theory the results collected in Fig. 4 and Table 4 clearly support that the polaronic motion observed by Laredo et al. in AgCl[25] actually involves Y - x^2-y^2 and X - x^2-z^2 hops.

A crucial question is to understand why these hops to next-nearest silver ions (R_S^* = 5.51 Å) have a smaller barrier than that for the XY - x^2-y^2 hop, where a nearest silver ion (R_S = 3.90 Å) is involved. This situation is, in principle, not easy to understand looking at the behavior of Slater-Koster parameters in transition metals[13]. Indeed, if R designates the distance between sites, the quantities $V_{dd\sigma}$ or $V_{dd\pi}$ are found to depend strongly on R, for transition metals being proportional

to R^{-5} [13]. Nevertheless, in AgCl when the hole resides around a silver site its charge is mainly lying not on silver but on the ligands of a $AgCl_6^{4-}$ complex. For this reason, in AgCl the S_{OY} = $\langle b_{1g}(O)|b_{1g}(Y)\rangle$ overlap, between the b_{1g} orbital at the origin, $b_{1g}(O)$, and that lying at Y, $b_{1g}(Y)$, is not only determined by $\langle x^2\text{-}y^2(O)|x^2\text{-}y^2(Y)\rangle$ involving the *distant* d-wavefunctions. Indeed, there is another contribution to S_{OY} and $V_{dd\sigma}$ solely associated with ligand wavefunctions described by Eq. (12). In order to clarify this relevant matter the shape of both $b_{1g}(O)$ and $b_{1g}(Y)$ molecular orbitals is portrayed in Fig. 5, where only the Cl(3p) orbitals are included in the ligand contribution. This admixture gives rise to a contribution to the S_{OY} overlap equal to $\beta_{p\sigma}^2\langle\chi_{p\sigma}(O)|\chi_{p\sigma}(Y)\rangle$ depending only on 3p(Cl) wavefunctions. Although, as shown in Eq. (12), there is also a contribution of 3s(Cl) orbitals to a b_{1g} molecular orbital it has been calculated $(\beta_s/\beta_{p\sigma})^2 \approx 0.05$ for $AgCl_6^{4-}$ [82-83]. This low value is consistent with the high covalency in the $AgCl_6^{4-}$ complex as an increase of covalency tends to reduce the $(\beta_s/\beta_{p\sigma})^2$ quantity[82-83, 85]. For this reason we shall discard in a first step the hybridization with 3s(Cl) orbitals for discussing the contribution of ligands to the S_{OY} overlap. Bearing this fact in mind we realise, looking at Fig. 5, that there is a *common* ligand, C, for $b_{1g}(O)$ and $b_{1g}(Y)$ orbitals. Moreover, the 3p(L) orbital corresponding to the bridging C ligand involved in $b_{1g}(O)$ and $b_{1g}(Y)$ orbitals is *the same*. This makes the ligand contribution to the S_{OY} overlap equal to $(\beta_{p\sigma}/2)^2$. This quantity, which is thus *independent* on the distance, R_S*, between the two involved sites, directly reflects the covalency *inside a single* $AgCl_6^{4-}$ unit as well as the relative orientation of $b_{1g}(O)$ and $b_{1g}(Y)$ orbitals.

It is worth noting now that a similar contribution to that found for the S_{OY} overlap *does not* appear when we consider a XY - x^2-y^2 hop involving a nearest silver ion at R_S = 3.90 Å. As it can be seen in Fig. 5 the two 3p orbitals on the bridging ligand are orthogonal thus implying $\langle\chi_{p\sigma}(O)|\chi_{p\sigma}(Y)\rangle = 0$ and a null contribution from ligands to S_{OY} and $V_{dd\pi}$. This explains, albeit qualitatively, why the barrier for the XY - x^2-y^2 short hop can be higher than that for the long Y - x^2-y^2 hop. Interestingly, if we consider the angle, ϕ, formed by the line joining the initial silver ion and the bridging ligand with that formed by this ligand and the final silver ion we see that $\phi = 0$ for the Y - x^2-y^2 and X - x^2-z^2 hops, while $\phi = \pi/2$ for XY - x^2-y^2 short hop. The present results thus stress that for the motion of the polaron in AgCl paths involving $\phi = 0$ are preferred over those with ϕ =

$\pi/2$. These conclusions are thus in tune with what happens for the superexchange interaction in cubic insulating lattices containing transition metal cations[87].

Using Eq. (11) and taking into account that the barrier for the $Y-x^2-y^2$ hop is 36 meV we can estimate that $\gamma_{x^2-y^2;x^2-y^2}(Y)$ = 200 meV. This value is in reasonable agreement with the one obtained from the analysis of the DFT Hamiltonian expressed in Wannier functions[79, 88-89] where the effective $\gamma_{x^2-y^2;x^2-y^2}(Y)$ value is found to be 290 meV. The Wannier analysis was made through an effective tight-binding Hamiltonian for the Ag(e_g) levels based on the full Ag(4d)+L(3p/4p) valence bands (See Fig. 5). We found that all interactions had the (negative) sign expected from simple arguments. This kind of analysis also allows us to find the $\gamma_{x^2-y^2;x^2-y^2}(Y)$ value in AgBr, 405 meV, which is 40% percent larger than the one corresponding to AgCl. This enlargement of γ is consistent with the lower localization of the hole in AgBr when compared to AgCl leading to the absence of self-trapping in the former lattice.

6. OPTICAL PROPERTIES OF THE SELF-TRAPPED HOLE IN AGCL

The results on section 4 and Table 1 have underlined the similarities between the spin Hamiltonian parameters of the STH in AgCl with those coming from Ag^{2+} impurities formed in NaCl and KCl host lattices. Accordingly, the comparison of optical absorption data of the STH in AgCl[21, 23, 27, 31] with those for KCl: Ag^{2+} [36]can shed light on the actual origin of the broad band peaked at 1.2 eV observed for the former system[21, 27, 31].

As shown in Table 9 the three crystal-field transitions have been observed for the $AgCl_6^{4-}$ complex formed in KCl[36]. The assignment of such transitions is well supported by first principle calculations[53] which reproduce reasonably well the experimental crystal-field and charge-transfer energies measured for KCl: Ag^{2+} [36]. The first charge-transfer transition for this system, that appears only at 2.70 eV as a result of the high optical electronegativity of Ag^{2+}[82-83], is lying above the $b_{1g}(x^2-y^2) \rightarrow e_g(xz,yz)$ transition[36, 53].

Among the three crystal-field transitions observed in KCl:Ag^{2+} $b_{1g}(x^2-y^2) \rightarrow a_{1g}(3z^2-r^2)$ has the smallest energy[36, 53]. As the energy of such a transition, denoted as $E(z^2)$, would be zero if the

octahedral $AgCl_6^{4-}$ complex is placed in a cubic lattice[90] it depends on the tetragonal distortion in the complex reflected in the $R_{ax} - R_{eq} = 3\varepsilon$ quantity. As in a JT system $E(z^2) \cong 4E_{JT}$ [41], we get from the calculations[53] carried out on $KCl:Ag^{2+}$ and $NaCl:Ag^{2+}$ $(1/3)[dE(z^2)/d\varepsilon] = 2$ eV/Å. As $E(z^2) = 1.55$ eV for $KCl:Ag^{2+}$, where $3\varepsilon = 0.45$ Å[36, 53], one can expect that if $3\varepsilon = 0.36$ Å, such as it has been calculated for the STH in AgCl, $E(z^2)$ should be around 1.37 eV. This figure is thus not far but a bit higher than the maximum of the optical absorption band experimentally observed for the STH in AgCl[21, 27]. It should be noted however that, contrary to what happens in $KCl:Ag^{2+}$, around 15% of the hole density is lying outside the $AgCl_6^{4-}$ complex for the STH in AgCl. In a way somewhat similar to what is found for the hyperfine tensor this delocalization would induce an additional reduction on the $E(z^2)$ transition energy. The present arguments thus strongly support that the peak experimentally observed at 1.2 eV for the STH in AgCl[21, 27, 31] can be assigned as the $b_{1g}(x^2-y^2) \rightarrow a_{1g}(3z^2-r^2)$ transition.

Interestingly, if, according to the present calculations, the ground state of the STH in AgCl lies 0.165 eV below the free hole state the excited $a_{1g}(3z^2-r^2)$ level should be about 1 eV *above* such state. This fact thus nicely explains why the concentration of STHs decreases when shinning in the infrared band peaked at 1.2 eV[21]. Moreover, the motion of free holes induced by this infrared light can lead to a luminescence arising from the recombination with trapped electrons. This luminescence is well observed in AgCl crystals doped with copper and grown in a chlorine atmosphere where self-trapped holes and electrons trapped as Cu^+ are both simultaneously formed[21, 27].

7. ABSENCE OF STH IN AGBR

Bearing the results conveyed in sections 4 and 5 in mind we have also explored whether a STH can also exist in the AgBr lattice which displays the same crystal structure as AgCl. At variance with our results in silver chloride, AgBr was found to be unable to support a localized hole, in good agreement with the experiments, where no STH has been observed in AgBr down to at least 1.7 K[18, 30]. Although in our calculations the system with an added hole was prepared in a favorable initial configuration, as it described in section 3 (i.e. starting from the geometry of a localized hole in a NaBr lattice doped with one single Ag ion), it always relaxed to a delocalized state solution.

In order to get an estimation of the relative energies of the B_{1g} and A_{1g} localized states with respect to the preferred delocalized state we utilized the following procedure. First, we scaled the JT distortions obtained for the STH in AgCl by the ratio between the AgBr and AgCl lattice parameters. Then, with the $AgBr_6^{4-}$complex kept fixed, the rest of the ions in the supercell were allowed to relax because, as already pointed out, if all ions are allowed to relax a delocalized solution is obtained for the hole in AgBr. By doing this, we obtain that the B_{1g} and A_{1g} states are 195 meV and 377 meV, respectively, less stable than the delocalized state.

At this point a crucial question arises: what is different in AgBr relative to AgCl that makes the STH possible in the latter but not in the former? This significant difference can hardly be due to an elastic energy gained during the trapping, E_{trap}, which is much larger in AgCl than in AgBr. Indeed the elastic properties of both materials are very similar as shown by the experimental bulk modulus of AgCl (53.6 GPa) and AgBr (50.6 GPa). By contrast, the different behavior of AgCl and AgBr for stabilizing a STH could be associated with the smaller gap in AgBr (2.68 eV) when compared to that of AgCl (3.25 eV). For exploring the reliability of this idea we performed a computational experiment in which we swapped the AgBr and AgCl band gaps. We did this by tuning the U parameters in such a way that AgCl had the direct and indirect band gaps of AgBr and viceversa. This is achieved by imposing $U_{\mathrm{Ag(s)}} = 2$ eV and $U_{\mathrm{Cl(p)}} = 2.5$ eV for AgCl and $U_{\mathrm{Ag(s)}} = 3.0$ eV and $U_{\mathrm{Br(p)}} = 7.0$ eV for AgBr. By doing this we obtained that if AgCl had the band gap of AgBr the hole would not be localized. On the other hand, if AgBr showed the band gap of AgCl the localized solution in the B_{1g} state would become 610 meV more stable than the delocalized solution, confirming the difference in the band gap of the two systems as the cause for having SHT in AgCl but not in AgBr.

The smaller gap in AgBr than in AgCl reflects the smaller electronegativity of bromine (2.8) when compared to that of chlorine (3.0) implying that covalence is higher in the former than in the latter compound. This fact together with the low value, $|E_b|$= 0.165eV, found for the STH in AgCl helps us to understand its absence in AgBr using the analysis carried out in section 5. It has been shown that the *lowest* barrier for polaron motion in AgCl takes place for Y - x^2-y^2 and X - x^2-z^2 hops. Moreover, such a barrier decreases when the covalency inside a *single* AgX_6^{4-} unit (X = halide), reflected in the $\beta_{p\sigma}^2$ quantity, raises. As on passing from $AgCl_6^{4-}$ to $AgBr_6^{4-}$ the covalency and thus

$\beta_{p\sigma}^2$ has to increase this fact tends to reduce the barrier found for AgCl favoring that the free hole can be more stable than the STH in AgBr. It is worth noting now that from EPR data obtained for $CdBr_2:Ag^{2+}$ [91] the covalency of an *isolated* $AgBr_6^{4-}$ unit has been estimated[92]. As a main conclusion of that analysis the value $\beta_{p\sigma}^2 \approx 0.9$ found for $AgBr_6^{4-}$, which is clearly higher than $\beta_{p\sigma}^2 \approx 0.6$ for $AgCl_6^{4-}$, implies a hole practically localized on ligands[92]. According to the present analysis, the absence of a STH in AgBr is thus greatly connected to the higher covalency in $AgBr_6^{4-}$ than in $AgCl_6^{4-}$, which in turn reflects the smaller electronegativity of bromine when compared to that of chlorine.

It is worth noting now that while in silver halides the STH is not stable in AgBr a quite different situation holds in alkali halides and alkali earth halides. In this sense, STH in the form of X_2^- centers (X = halide) are formed, for instance, in NaF[12], NaCl[33, 93], $BaCl_2$ [94], $SrCl_2$[95], NaBr[12, 93] and $BaBr_2$ [96] as a result of a valence band mainly made of *np* halide orbitals. As the X_2^- radicals are homonuclear species the electronic charge is *equally* shared by the two involved atoms and thus this happens for Cl_2^- centers formed in NaCl as well as for Br_2^- centers formed in NaBr. By contrast, AgX_6^{4-} species (X = Cl, Br) are *heteronuclear* molecules where the electronic charge lying on a ligand depends drastically on its nature a fact that, as it has been shown, has an important influence upon the stability of the STH in silver halides.

8. FINAL REMARKS

The present results obtained on the *model* compounds AgCl and AgBr shed light on the stability and motion of small polarons. In this sense the calculations carried out in this work show that STH can spontaneously be formed in AgCl although E_b = -0.165eV is one order of magnitude smaller than that corresponding to the Cl_2^- center in KCl[12, 16]. By contrast, in agreement with experimental results[18, 30], the present calculations support that no STH can be formed in AgBr , a fact helped by the higher covalency induced by the substitution of chlorine by bromine. The study carried out in this work also proves that Y - x^2-y^2 and X - x^2-z^2 hops are essentially responsible for the polaron migration in AgCl. Interestingly, a hop like X - x^2-z^2 makes possible that a STH which is initially placed in XY plane can reach another equivalent plane. Moreover, if the dominant mechanism for polaron motion is through Y - x^2-y^2 and X - x^2-z^2 hops, this means that a STH placed

at the beginning at (0,0,0) can easily move along the *sublattice* of silver sites described by $\boldsymbol{\tau} = a(m\mathbf{i} + n\mathbf{j} + p\mathbf{k})$ where a is the lattice parameter and m, n and p are integers. By contrast, it is more difficult for the polaron to reach silver sites corresponding to the other cubic sublattices starting in (a/2, a/2, 0), (a/2, 0, a/2) and (0, a/2, a/2).

Let us designate by $|h_n\rangle$ the wavefunction of a STH localized in the n site of the AgCl lattice. As in a *perfect* AgCl lattice all the silver sites are in principle equivalent the actual ground state wavefunction would involve a linear combination of all $|h_n\rangle$ (n = 1, 2,..., N) localized wavefunctions, thus implying the existence of a *coherent* tunneling. Nevertheless, this situation is not experimentally observed due to the unavoidable presence of defects in any real crystal which break such a coherence and favor the localization of the hole at a given site. Accordingly, the subsequent motion of the polaron involves an *incoherent* hopping to close silver sites. This situation is thus somewhat similar to that found for excitons in pure insulating compounds like MnF_2 or Cr_2O_3 [97]. Upon illumination with visible light a transition-metal cation in an excited state is created at a given point of the lattice. This excitation can migrate through *incoherent* hops along the lattice and thus can be trapped by an unwanted impurity[97]. If in this case the excitation decay is dominated by a non-radiative process and the luminescence in the pure compound is quenched such as it happens for Cr_2O_3 contrary to what is found in *diluted* ruby (Al_2O_3:Cr^{3+}) where the excitation at Cr^{3+} is unable to migrate. Along this line also the observation of a static Jahn–Teller effect in cases like KCl:Ag^{2+} cannot be explained without the presence of random strains due to defects as they determine the principal C_4 axis at a given point of the lattice[50-51].

Similarly to what is found for alkali halides experimental results prove that electrons in the conduction band of silver halides are not self-trapped but can move freely[22, 98]. Nevertheless, such electrons move *together with* the associated lattice polarization thus giving rise to a long range polaron whose mass, m_p, is higher than the effective mass, m*, for the conduction band, m_p/m^* being around 1.3 for both AgCl and AgBr[22, 98]. Interestingly, the size of the large polaron is given by $(\hbar/2m^*\omega_L)^{1/2}$, where ω_L denotes the longitudinal optical frequency[11, 14]. This expression, using m* = 0.215m and $\omega_L = 3.66\ 10^{13}$ rad, leads to an extension of the large polaron around 30 Å for AgCl[98] which is thus an order of magnitude higher than that for the STH.

Although electrons placed in the conduction band of alkali and silver halides are not self-trapped this is not a general rule for insulating materials[9, 99-100]. In particular, experimental results by Nistor et al.[99] strongly support the formation of self-trapped electrons in X-irradiated $PbCl_2$. To understand why electron self-trapping occurs in this compound is certainly a relevant question to be answered. Work along this line in now underway.

AUTHOR INFORMATION

Corresponding Author

***E-mail: jmgla@dtu.dk.**

***Telephone number: +45 93511632**

Notes

The authors declare no competing financial interest.

ACKNOWLEDGEMENTS

Support by the Spanish Ministry of Economy and Competitiveness under Project FIS2012-30996 is acknowledged. J.M.G.L. acknowledges support from the same source under Project FIS2013-46159-C3-1-P and from the Villum Foundation's Young Investigator Programme (4th round, project: *In silico design of efficient materials for next generation batteries.* Grant number: 10096). P.G.F. acknowledges support through the Ramon y Cajal fellowship with reference RYC-2013-12515.

REFERENCES

1. Landau, L. D., Über die Bewegung der Elektronen in Kristallgitter. *Physik Z. Sowjetunion* **1933,** *3*, 644-645.

2. Emin, D., *Polarons*. Cambridge University Press: New York, 2013.

3. Bussmann-Holder, A.; Keller, H., Polaron Effects in High-Temperature Cuprate Superconductors. In *Polarons in Advanced Materials*, Alexandrov, A. S., Ed. Springer: 2007.

4. Millis, A. J., Lattice Effects in Magnetoresistive Manganese Perovskites. *Nature* **1998,** *392* (6672), 147-150.

5. Dagotto, E.; Hotta, T.; Moreo, A., Colossal Magnetoresistant Materials: The Key Role of Phase Separation. *Phys. Rep.-Rev. Sec. Phys. Lett.* **2001,** *344* (1-3), 1-153.

6. Romero, E.; Augulis, R.; Novoderezhkin, V. I.; Ferretti, M.; Thieme, J.; Zigmantas, D.; van Grondelle, R., Quantum Coherence in Photosynthesis for Efficient Solar-Energy Conversion. *Nature Physics* **2014,** *10* (9), 677-683.

7. Kim, J.; Unterreiner, A. N.; Rane, S.; Park, S.; Jureller, J.; Book, L.; Liau, Y. H.; Scherer, N. F., Ultrafast Dephasing of Photoexcited Polarons in Primary Doped Polyaniline. *Journal of Physical Chemistry B* **2002,** *106* (50), 12866-12873.

8. Bassler, H.; Kohler, A., Charge Transport in Organic Semiconductors. In *Unimolecular and Supramolecular Electronics I: Chemistry and Physics Meet at Metal-Molecule Interfaces*, Metzger, R. M., Ed. 2012; Vol. 312, pp 1-65.

9. Garcia-Lastra, J. M.; Myrdal, J. S. G.; Christensen, R.; Thygesen, K. S.; Vegge, T., DFT plus U Study of Polaronic Conduction in Li_2O_2 and Li_2CO_3: Implications for Li-Air Batteries. *Journal of Physical Chemistry C* **2013,** *117* (11), 5568-5577.

10. Austin, I. G.; Mott, N. F., Polarons in Crystalline and Non-Crystalline Materials. *Advances in Physics* **1969,** *18* (71), 41-&.

11. Fröhlich, H., Electrons in Lattice Fields. *Advances in Physics* **1954,** *3* (11), 325-361.

12. Fowler, W. B., *Physics of Color Centers*. Academic Press: 1968.

13. Harrison, W. A., *Electronic Structure and the Properties of Solids: The Physics of the Chemical Bond*. Dover Publications: 2012.

14. Lee, T. D.; Low, F. E.; Pines, D., The Motion of Slow Electrons in a Polar Crystal. *Physical Review* **1953,** *90* (2), 297-302.

15. Holstein, T., Studies of Polaron Motion 2. The Small Polaron. *Annals of Physics* **1959,** *8* (3), 343-389.

16. Jette, A. N.; Gilbert, T. L.; Das, T. P., Theory of Self-Trapped Hole in Alkali Halides. *Physical Review* **1969,** *184* (3), 884-&.

17. Baranov, P. G.; Romanov, N. G.; Poluektov, O. G.; Schmidt, J., Self-Trapped Excitons in Ionic-Covalent Silver Halide Crystals and Nanostructures: High-Frequency EPR, ESE, ENDOR and ODMR Studies. *Applied Magnetic Resonance* **2010,** *39* (4), 453-486.

18. Baxter, J. E.; Ascarell.G, Temperature-Dependence of Cyclotron-Resonance Absorption of Electrons in AgBr. *Physica Status Solidi B-Basic Research* **1974,** *62* (2), 547-558.

19. Bennebroek, M. T. Ph.D. Thesis: High-Field Electron Nuclear Double Resonance Spectroscopy on Photo-Induced Centers in Silver Halides. University of Leiden, 1996.

20. Carrera, N. J.; Brown, F. C., Optical Response of AgCl And AgBr nn Near and Extreme Ultraviolet. *Physical Review B* **1971,** *4* (10), 3651-&.

21. Fukui, M.; Hayashi, Y.; Yoshioka, H., ESR Study of Growth and Decay Processes of Self-Trapped Holes in Agcl Crystals Doped With Cu. *Journal of the Physical Society of Japan* **1973,** *34* (5), 1226-1233.

22. Hodby, J. W.; Borders, J. A.; Brown, F. C.; Foner, S., Cyclotron Resonance of Polaron in KCl, KBr, KI, RbCl, AgCl, AgBr, and TlCl. *Physical Review Letters* **1967,** *19* (17), 952-&.

23. Hohne, M.; Stasiw, M., ESR Detection of Self-Trapped Holes in Agcl. *Physica Status Solidi* **1968,** *28* (1), 247-&.

24. Kanzaki, H.; Sakuragi, S., Optical Absorption and Luminescence of Excitons in Silver Halides Containing Isoelectronic Impurities .2. AgBr-Cl- and AgBr. *Journal of the Physical Society of Japan* **1970,** *29* (4), 924-&.

25. Laredo, E.; Paul, W. B.; Rowan, L.; Slifkin, L., Interactions between Self-Trapping and Solute Trapping of Photocarriers in Pd-Doped AgCl. *Physical Review B* **1983,** *27* (4), 2470-2476.

26. Laredo, E.; Rowan, L. G.; Slifkin, L., Energy Barrier Against Self-Trapping of the Hole in Silver-Chloride. *Physical Review Letters* **1981,** *47* (5), 384-387.

27. Marquard.Cl; Williams, R. T.; Kabler, M. N., Hole Self Trapping and Recombination Luminescence in Agl at Low Temperatures. *Solid State Communications* **1971,** *9* (24), 2285-&.

28. Slifkin, L., Dynamics of Self-Trapped Hole Processes in AgCl. *Journal of Physics-Condensed Matter* **2001,** *13* (10), 2347-2353.

29. Song, A. K. S.; Williams, R. T., *Self-Trapped Excitons*. Springer: 1996.

30. Tamura, H.; Masumi, T., Cyclotron-Resonance of Positive Holes in AgBr. *Solid State Communications* **1973,** *12* (11), 1183-1186.

31. Yoshioka, H.; Yamaga, M., Molecular-Orbitals of the Self-Trapped Holes and The Zero-Field Splitting of the Self-Trapped Excitons in AgCl Crystals. *Journal of the Physical Society of Japan* **1985,** *54* (2), 841-848.

32. Mott, N. F.; Gurney, R. W., *Electronic Processes in Ionic Crystals*. Oxford: Clarendon Press: Oxford, 1940.

33. Castner, T. G.; Kanzig, W., The Electronic Structure of V-Centers. *Journal of Physics and Chemistry of Solids* **1957,** *3* (3-4), 178-195.

34. Gazzinel.R; Mieher, R. L., Electron-Nuclear Double Resonance of Self-Trapped Hole in LiF. *Physical Review* **1968,** *175* (2), 395-&.

35. Bennebroek, M. T.; van Duijn-Arnold, A.; Schmidt, J.; Poluektov, O. G.; Baranov, P. G., Self-Trapped Hole in Silver Chloride Crystals: A Pulsed PR/ENDOR Study at 95 GHz. *Physical Review B* **2002,** *66* (5), 054305.

36. Delbecq, C. J.; Obrien, M. C. M.; Yuster, P. H.; Hayes, W., Paramagnetic Resonance and Optical Absorption of Trapped Holes and Electrons in Irradiated KCl:Ag. *Proc. R. Soc. Lond. A-Math. Phys. Sci.* **1963,** *271* (1344), 243-+.

37. Sierro, J., Paramagnetic Resonance of the Ag^{2+} Ion in Irradiated Alkali Chlorides. *Journal of Physics and Chemistry of Solids* **1967,** *28* (3), 417-422.

38. *We follow the standard notation for doped solids, i.e. NaCl:Ag^{2+} stands for Sodium Chloride doped with trace amounts of Ag^{2+} ions.*

39. Holstein, T., Studies of Polaron Motion 1. The Molecular-Crystal Model. *Annals of Physics* **1959,** *8* (3), 325-342.

40. Devreese, J. T., *Polarons in Ionic Crystals and Polar Semiconductors: Antwerp Advanced Study Institute 1971 on Fröhlich Polarons and Electron-Phonon Interaction in Polar Semiconductors*. North-Holland Pub. Co.: 1972.

41. Bersuker, I. B., *The Jahn-Teller Effect*. Cambridge University Press: 2006.

42. Ramanantoanina, H.; Zlatar, M.; Garcia-Fernandez, P.; Daul, C.; Gruden-Pavlovic, M., General Treatment of the Multimode Jahn-Teller Effect: Study of Fullerene Cations. *Physical chemistry chemical physics : PCCP* **2013,** *15* (4), 1252-9.

43. Garcia-Fernandez, P.; Sousa, C.; Aramburu, J. A.; Barriuso, M. T.; Moreno, M., Coherent Tunneling in Cu^{2+}- And Ag^{2+}-Doped MgO and CaO : Cu^{2+} Explored Through Ab Initio Calculations. *Physical Review B* **2005,** *72* (15).

44. Brik, M. G.; Ogasawara, K., Microscopic Analysis of the Crystal Field Strength and Lowest Charge Transfer Energies in The Elpasolite Crystals Cs_2NaYX_6 (X=F, Cl, Br) Doped with Cr^{3+}. *Physical Review B* **2006,** *74* (4).

45. Garcia-Lastra, J. M.; Moreno, M.; Barriuso, M. T., Pressure Effects on $CrCl_6^{3-}$ Embedded in Cubic Cs_2NaMCl_6 (M=Sc, Y) Lattices: Study Through Periodic and Cluster Calculations. *Journal of Chemical Physics* **2008,** *128* (14).

46. Garcia-Lastra, J. M.; Wesolowski, T.; Barriuso, M. T.; Aramburu, J. A.; Moreno, M., Optical and Vibrational Properties of MnF_6^{4-} Complexes in Cubic Fluoroperovskites: Insight through Embedding Calculations Using Kohn-Sham Equations with Constrained Electron Density. *Journal of Physics-Condensed Matter* **2006,** *18* (5), 1519-1534.

47. Tanner, P. A., Fluorescence and Phosphorescence of Cr^{3+}in Cubic Hosts. *Chemical Physics Letters* **2004,** *388* (4-6), 488-493.

48. Wenger, O. S.; Gudel, H. U., Optical Spectroscopy of $CrCl_6^{3-}$ Doped $Cs_2NaScCl_6$: Broadband Near-Infrared Luminescence and Jahn-Teller Effect. *Journal of Chemical Physics* **2001,** *114* (13), 5832-5841.

49. Zener, C., Interaction between the *d*-Shells in the Transition Metals. II. Ferromagnetic Compounds of Manganese with Perovskite Structure. *Physical Review* **1951,** *82* (3), 403-405.

50. Garcia-Fernandez, P.; Trueba, A.; Barriuso, M. T.; Aramburu, J. A.; Moreno, M., Dynamic and Static Jahn-Teller Effect in Impurities: Determination of the Tunneling Splitting. In *Vibronic Interactions and the Jahn-Teller Effect: Theory and Applications*, Atanasov, M.; Daul, C.; TregennaPiggott, P. L. W., Eds. 2012; Vol. 23, pp 105-142.

51. Ham, F. S., Jahn-Teller Effects in EPR spectra. In *Electron Paramagnetic Resonance*, Geschwind, S., Ed. Plenum: New York, 1972.

52. Slater, J. C.; Koster, G. F., Simplified LCAO Method for the Periodic Potential Problem. *Physical Review* **1954,** *94* (6), 1498-1524.

53. Trueba, A.; Garcia-Lastra, J. M.; de Graaf, C.; Garcia-Fernandez, P.; Barriuso, M. T.; Aramburu, J. A.; Moreno, M., Jahn-Teller Effect in Ag^{2+} Doped KCl and NaCl: Is There any Influence of the Host Lattice? *Chemical Physics Letters* **2006,** *430* (1-3), 51-55.

54. Anisimov, V. I.; Aryasetiawan, F.; Lichtenstein, A. I., First-Principles Calculations of the Electronic Structure and Spectra of Strongly Correlated Systems: The LDA+U Method. *Journal of Physics-Condensed Matter* **1997,** *9* (4), 767-808.

55. Dudarev, S. L.; Liechtenstein, A. I.; Castell, M. R.; Briggs, G. A. D.; Sutton, A. P., Surface States on NiO (100) and the Origin of the Contrast Reversal in Atomically Resolved Scanning Tunneling Microscope Images. *Physical Review B* **1997,** *56* (8), 4900-4908.

56. Cococcioni, M.; de Gironcoli, S., Linear Response Approach to the Calculation of the Effective Interaction Parameters in the LDA+U Method. *Physical Review B* **2005,** *71* (3), 035105.

57. *The U parameter used in this paper refers to the (U-J) parameter in the original DFT+U formulation*.

58. Bengone, O.; Alouani, M.; Blochl, P.; Hugel, J., Implementation of the Projector Augmented-Wave LDA+U Method: Application to the Electronic Structure of NiO. *Physical Review B* **2000,** *62* (24), 16392-16401.

59. Finazzi, E.; Di Valentin, C.; Pacchioni, G.; Selloni, A., Excess Electron States in Reduced Bulk Anatase TiO_2: Comparison of Standard GGA, GGA Plus U, and Hybrid DFT Calculations. *Journal of Chemical Physics* **2008,** *129* (15), 154113.

60. Mosey, N. J.; Carter, E. A., Ab Initio Evaluation of Coulomb and Exchange Parameters for DFT+U Calculations. *Physical Review B* **2007,** *76* (15), 155123.

61. Droghetti, A.; Pemmaraju, C. D.; Sanvito, S., Polaronic Distortion and Vacancy-Induced Magnetism in MgO. *Physical Review B* **2010,** *81* (9), 092403.

62. Nolan, M.; Watson, G. W., Hole Localization in Al Doped Silica: A DFT+U Description. *Journal of Chemical Physics* **2006,** *125* (14), 144701.

63. Slipukhina, I.; Mavropoulos, P.; Blugel, S.; Lezaic, M., Ferromagnetic Spin Coupling of 2p Impurities in Band Insulators Stabilized by an Intersite Coulomb Interaction: Nitrogen-Doped MgO. *Physical Review Letters* **2011,** *107* (13), 137203.

64. Wu, Z. G.; Cohen, R. E., More Accurate Generalized Gradient Approximation for Solids. *Physical Review B* **2006,** *73* (23).

65. Perdew, J. P.; Ruzsinszky, A.; Csonka, G. I.; Vydrov, O. A.; Scuseria, G. E.; Constantin, L. A.; Zhou, X.; Burke, K., Restoring the Density-Gradient Expansion for Exchange in Solids and Surfaces. *Physical Review Letters* **2008,** *100* (13), 136406.

66. Garcia-Fernandez, P.; Ghosh, S.; English, N. J.; Aramburu, J. A., Benchmark Study for the Application of Density Functional Theory to the Prediction of Octahedral Tilting in Perovskites. *Physical Review B* **2012,** *86* (14), 144107.

67. Enkovaara, J.; Rostgaard, C.; Mortensen, J. J.; Chen, J.; Dulak, M.; Ferrighi, L.; Gavnholt, J.; Glinsvad, C.; Haikola, V.; Hansen, H. A., et al., Electronic Structure Calculations with GPAW: a Real-Space Implementation of the Projector Augmented-Wave Method. *Journal of Physics-Condensed Matter* **2010,** *22* (25), 253202.

68. Bahn, S. R.; Jacobsen, K. W., An Object-Oriented Scripting Interface to aLegacy Electronic Structure Code. *Computing in Science & Engineering* **2002,** *4* (3), 56-66.

69. Perdew, J. P.; Burke, K.; Ernzerhof, M., Generalized Gradient Approximation Made Simple. *Physical Review Letters* **1996,** *77* (18), 3865-3868.

70. Wilson, D. J.; Sokol, A. A.; French, S. A.; Catlow, C. R. A., Defect Structures in The Silver Halides. *Physical Review B* **2008,** *77* (6), 064115.

71. Perdew, J. P.; Wang, Y., Accurate and Simple Analytic Representation of the Electron-Gas Correlation-Energy. *Physical Review B* **1992,** *45* (23), 13244-13249.

72. Benmessabih, T.; Amrani, B.; Hassan, F. E. H.; Hamdache, F.; Zoaeter, M., Computational Study of AgCl and AgBr Semiconductors. *Physica B-Condensed Matter* **2007,** *392* (1-2), 309-317.

73. Stephens, P. J.; Devlin, F. J.; Chabalowski, C. F.; Frisch, M. J., Ab-Initio Calculation of Vibrational Absorption and Circular-Dichroism Spectra Using Density-Functional Force-Fields. *Journal of Physical Chemistry* **1994,** *98* (45), 11623-11627.

74. Rathor, A.; Arora, G.; Ahuja, B. L., Band-Structure Calculations and Electron Momentum Densities of AgCl and AgBr. *Physica Status Solidi B-Basic Solid State Physics* **2008,** *245* (8), 1563-1570.

75. Vogel, D.; Kruger, P.; Pollmann, J., Ab Initio Electronic Structure of Silver Halides Calculated with Self-Interaction and Relaxation-Corrected Pseudopotentials. *Physical Review B* **1998,** *58* (7), 3865-3869.

76. Henkelman, G.; Uberuaga, B. P.; Jonsson, H., A Climbing Image Nudged Elastic Band Method for Finding Saddle Points and Minimum Energy Paths. *Journal of Chemical Physics* **2000,** *113* (22), 9901-9904.

77. Ong, S. P.; Mo, Y.; Ceder, G., Low Hole Polaron Migration Barrier in Lithium Peroxide. *Physical Review B* **2012,** *85* (8), 081105

78. Wang, Z.; Bevan, K. H., Exploring the Impact of Semicore Level Electronic Relaxation on Polaron Dynamics: An Adiabatic Ab Initio Study of $FePO_4$. *Physical Review B* **2016,** *93* (2), 024303.

79. Mostofi, A. A.; Yates, J. R.; Lee, Y.-S.; Souza, I.; Vanderbilt, D.; Marzari, N., Wannier90: A Tool for Obtaining Maximally-Localised Wannier Functions. *Computer Physics Communications* **2008,** *178* (9), 685-699.

80. Kresse, G.; Furthmuller, J., Efficient Iterative Schemes for Ab Initio Total-Energy Calculations Using a Plane-Wave Basis Set. *Physical Review B* **1996,** *54* (16), 11169-11186.

81. Heyd, J.; Scuseria, G. E.; Ernzerhof, M., Hybrid Functionals Based on a Screened Coulomb Potential. *Journal of Chemical Physics* **2003,** *118* (18), 8207-8215.

82. Aramburu, J. A.; Moreno, M., Bonding of Ag^{2+} in KCl Lattice. *Solid State Communications* **1986,** *58* (5), 305-309.

83. Valiente, R.; Aramburu, J. A.; Barriuso, M. T.; Moreno, M., Electronic-Structure of Ag^{2+} Impurities in Halide Lattices. *Journal of Physics-Condensed Matter* **1994,** *6* (24), 4515-4525.

84. Jørgensen, C. K., Electron Transfer Spectra. In *Progress in Inorganic Chemistry*, John Wiley & Sons, Inc.: 1970; pp 101-158.

85. Trueba, A.; Garcia-Fernandez, P.; Garcia-Lastra, J. M.; Aramburu, J. A.; Barriuso, M. T.; Moreno, M., Spectrochemical Series and the Dependence of Racah and 10Dq Parameters on the Metal-Ligand Distance: Microscopic Origin. *Journal of Physical Chemistry A* **2011,** *115* (8), 1423-1432.

86. Marcus, R. A., Electron-Transfer Reactions in Chemistry - Theory and Experiment. *Reviews of Modern Physics* **1993,** *65* (3), 599-610.

87. Hay, P. J.; Thibeault, J. C.; Hoffmann, R., Orbital Interactions in Metal Dimer Complexes. *Journal of the American Chemical Society* **1975,** *97* (17), 4884-4899.

88. Marzari, N.; Mostofi, A. A.; Yates, J. R.; Souza, I.; Vanderbilt, D., Maximally Localized Wannier Functions: Theory and Applications. *Reviews of Modern Physics* **2012,** *84* (4).

89. Souza, I.; Marzari, N.; Vanderbilt, D., Maximally localized Wannier functions for entangled energy bands. *Physical Review B* **2002,** *65* (3).

90. Garcia-Fernandez, P.; Teresa Barriuso, M.; Garcia-Lastra, J. M.; Moreno, M.; Antonio Aramburu, J., Compounds Containing Tetragonal Cu^{2+} Complexes: Is the d_{x2-y2}-d_{3z2-r2} Gap a Direct Reflection of the Distortion? *Journal of Physical Chemistry Letters* **2013,** *4* (14), 2385-2390.

91. Miyanaga, T., EPR Studies of Strong Jahn-Teller Coupling Systems $CdCl_2$:Ag^{2+} And $CdBr_2$:Ag^{2+}. *Journal of the Physical Society of Japan* **1979,** *46* (1), 167-175.

92. Aramburu, J. A.; Moreno, M., The Anomalous Quasi Isotropic g Tensor Found for $CdBr_2$:Ag^{2+} And $AgBr_{0.15}Cl_{0.85}$:Ag^{2+} : An Explanation through Strong Covalency. *Solid State Communications* **1987,** *62* (7), 513-516.

93. Schoemak.D, g And Hyperfine Components of V_k Centers. *Physical Review B* **1973,** *7* (2), 786-801.

94. Houlier, B., EPR-Spectra of Color-Centers in X-Irradiated $BaCl_2$:K^+ and $BaCl_2$:Ag^+. *Solid State Communications* **1975,** *17* (3), 263-266.

95. Bill, H.; Suter, H.; Lacroix, R., V_K Center in $SrCl_2$ Crystals. *Physics Letters* **1966,** *22* (3), 241-&.

96. Moreno, M., EPR Study of a Hole-Center in $BaBr_2$:K. *Solid State Communications* **1975,** *16* (10-1), 1239-1241.

97. Wilson, B. A.; Yen, W. M.; Hegarty, J.; Imbusch, G. F., Luminescence from Pure MnF_2 and from MnF_2 Doped with Eu^{3+} and Er^{3+}. *Physical Review B* **1979,** *19* (8), 4238-4250.

98. Brown, F. C.; Dart, F. E., Electron Mobility in AgCl. *Physical Review* **1957,** *108* (2), 281-284.

99. Nistor, S. V.; Goovaerts, E.; Schoemaker, D., Direct Observation of Electron Self-Trapping in $PbCl_2$ Crystals. *Physical Review B* **1993,** *48* (13), 9575-9580.

100. Yang, S.; Brant, A. T.; Giles, N. C.; Halliburton, L. E., Intrinsic Small Polarons in Rutile TiO_2. *Physical Review B* **2013,** *87* (12).

101. Loje, K. F.; Schuele, D. E., Pressure and Temperature Derivatives of Elastic Constants of AgBr and AgCl. *Journal of Physics and Chemistry of Solids* **1970,** *31* (9), 2051-&.

102. Hidshaw, W.; Lewis, J. T.; Briscoe, C. V., Elastic Constants of Silver Chloride From 4.2 to 300 Degrees K. *Physical Review* **1967,** *163* (3), 876-&.

103. Berry, C. R., Physical Defects in Silver Halides. *Physical Review* **1955,** *97* (3), 676-679.

104. Blochl, P. E., Projector Augmented-Wave Method. *Physical Review B* **1994,** *50* (24), 17953-17979.

Tables

Table 1. Spin hamiltonian parameters measured for NaCl: Ag^{2+} and KCl: Ag^{2+} compared to those for the STH in AgCl. $A_{\|}$ and $A_{\perp}$ refer to silver hyperfine constants corresponding to the average isotope following the natural abundance of ^{107}Ag and ^{109}Ag while A_s and A_p describe the isotropic and anisotropic superhyperfine constants referred to an average chlorine isotope.

System	$g_{\|}$	$g_{\perp}$	$A_{\|}$ (MHz)	$A_{\perp}$ (MHz)	A_s (MHz)	A_p (MHz)	Ref.
STH in AgCl	2.147	2.040	93.1	61.3	30.1	24	[19, 35]
NaCl:Ag^{2+}	2.196	2.041	116±6	90±6	40±6	25±4	[37]
KCl:Ag^{2+}	2.193	2.035	122.7±1.5	90.9±1.5	42.5±3	27.5±2	[36-37]

Table 2. Slater-Koster parameters[52] for expressing the inter-site parameters, γ, for the cases shown in Fig. 2b. V and V* refer to nearest and next-nearest silver ions, respectively.

	$\gamma_{3z^2-r^2,3z^2-r^2}$	$\gamma_{3z^2-r^2,x^2-y^2}$	$\gamma_{x^2-y^2,x^2-y^2}$
Z	$V^*_{dd\sigma}$	0	$V^*_{dd\delta}$
X/Y	$\frac{1}{4}V^*_{dd\sigma}+\frac{3}{4}V^*_{dd\delta}$	$-\frac{\sqrt{3}}{4}V^*_{dd\sigma}+\frac{1}{4}V^*_{dd\delta}$	$\frac{3}{4}V^*_{dd\sigma}+\frac{1}{4}V^*_{dd\delta}$
XZ/YZ	$\frac{1}{16}\{V_{dd\sigma}+12V_{dd\pi}+3V_{dd\delta}\}$	$\frac{1}{16}\{\sqrt{3}V_{dd\sigma}-4V_{dd\pi}+3V_{dd\delta}\}$	$\frac{1}{16}\{3V_{dd\sigma}+4V_{dd\pi}+9V_{dd\delta}\}$
XY	$\frac{1}{4}V_{dd\sigma}+\frac{3}{4}V_{dd\delta}$	0	$V_{dd\pi}$

Table 3. Equivalent hops of hole polaron in AgCl. The first hop in each slot is the one referred to in the paper. Only the equivalences between hops along the positive axis are shown.

$XZ-x^2-y^2$	$YZ-x^2-y^2$		
$XY-x^2-y^2$			
$XZ-x^2-z^2$	$YZ-y^2-z^2$	$YZ-x^2-z^2$	$XY-y^2-z^2$
$XZ-y^2-z^2$	$YZ-x^2-z^2$		
$Y-x^2-y^2$	$X-x^2-y^2$		
$Z-x^2-y^2$			
$Z-x^2-z^2$	$Z-y^2-z^2$	$X-y^2-z^2$	$Y-x^2-z^2$
$X-x^2-z^2$	$Y-y^2-z^2$		

Table 4. Expressions of inter-site matrix elements corresponding to the eight non-equivalent hops in terms of the Slater-Koster parameters. V and V* refer to nearest and next-nearest silver ions placed along <110>and <100> directions respectively. The value of the barrier, *B*, calculated for the different hops is also enclosed.

Hop	γ	B (meV)
$XZ-x^2-y^2$	$\frac{1}{16}\{3V_{dd\sigma}+4V_{dd\pi}+9V_{dd\delta}\}$	198
$XY-x^2-y^2$	$-V_{dd\pi}$	92
$XZ-x^2-z^2$	$-\frac{V_{dd\pi}}{2}$	179
$XZ-y^2-z^2$	$\frac{1}{16}\{3V_{dd\sigma}-4V_{dd\pi}+9V_{dd\delta}\}$	185
$Y-x^2-y^2$	$\frac{3}{4}V^*_{dd\sigma}+\frac{1}{4}V^*_{dd\delta}$	36
$Z-x^2-y^2$	$V^*_{dd\delta}$	185
$Z-x^2-z^2$	$\frac{V^*_{dd\delta}}{2}$	193
$X-x^2-z^2$	$\frac{3}{4}V^*_{dd\sigma}-\frac{1}{4}V^*_{dd\delta}$	38

Table 5. Comparison between calculated and experimental properties of AgCl and AgBr. Experimental bulk moduli of AgCl and AgBr correspond to zero-temperature static values extrapolated from the data of Ref. [101]. Lattice parameter, a, of AgCl corresponds to zero-temperature static values extrapolated from the data of ref. [102]. B3LYP calculations from Ref. [74] do not optimize lattice parameters but taken those from Ref. [72].

System	Functional	$U_{Ag(s)}$	$U_{Cl(p)/Br(p)}$	Direct gap [eV]		Indirect gap [eV]		a [Å]		Bulk modulus [GPa]	
				Calc.	Exp.	Calc.	Exp.	Calc.	Exp.	Calc.	Exp.
AgCl	PBESol	4.0	5.0	5.09	5.15[20]	3.28	3.25[24]	5.494	5.51[102]	54.7	53.6[101]
	WC	4.0	5.0	5.07		3.25		5.490		51.2	
	PBE[70]	---	---	4.22		0.94		5.53		50.4	
	PW[72]	---	---	3.09		0.94		5.617		43.3	
	LDA-SIC[75]	---	---	4.5		2.3		5.53		60.7	
	B3LYP[74]	---	---	4.91		3.15		---		---	
AgBr	PBESol	5.25	3.0	4.27	4.30[20]	2.67	2.68[24]	5.802	5.77[103]	43.7	50.6[101]
	WC	5.25	3.0	4.24		2.63		5.794		41.1	
	PBE[70]	---	---	3.87		0.71		5.82		40.2	
	PW[72]	---	---	2.43		0.68		5.844		39.15	
	LDA-SIC[75]	---	---	3.1		1.6		5.71		---	
	B3LYP[74]	---	---	5.00		3.26		---		---	

Table 6: Calculated parameters for the localized B_{1g} and A_{1g} states in AgCl. R_L means the Ag^+-Cl^- distance of the perfect AgCl lattice. R_0 and ε describe the local lattice relaxation due to the $Ag^+ \rightarrow Ag^{2+}$ conversion. The energy of localized B_{1g} and A_{1g} states with respect to the state where the hole is fully delocalized is also given.

	R_L (Å)	R_0 [Å]	ε [Å]	Energy wrt delocalized state (meV)
B_{1g} (elongated)	2.76	2.61	0.119	-165
A_{1g} (compressed)	2.76	2.65	0.058	-109

Table 7. Magnitude of magnetic moments of ions shown in Fig. 1 obtained from DFT calculations performed in this study and experimental values (sum of the s- and d-orbital contributions)[35]. The DFT values have been calculated using PAW projectors and all-electron PAW basis functions to calculate weight factors for the site projected wave functions following the procedure described in Ref.[104]

Lattice site	**Magnetic moment μ_B units**	
	DFT (this study)	**EPR/ENDOR[35]**
Center Ag ion	0.1697	0.1930
X and Y Ag ion	0.0127	0.0156
Z Ag ion	0.0	0.0009
xy-plane Cl ion	0.1864	0.1630
Cl ion on elongation axis, neighboring center Ag ion	0.0068	0.0009
XY Ag ion	0.0002	0.0004
XZ Ag ion	0.0004	Not stated
XYZ Cl ion	0.0015	0.0002

Table 8. Comparison of the local relaxation, E_{trap} and E_b energies derived in this work for the STH in AgCl with those reported for the Cl_2^- center in KCl[12, 16].

System	Local relaxation	E_{trap}(eV)	E_b(eV)
Cl_2^- in KCl	$R_L - R$ = 1.49 Å	~-1.5	-1.5
STH in AgCl	$R_L - R_{ax}$ = -0.09 Å ; $R_L - R_{eq}$ = 0.27 Å	-0.47	-0.165

Table 9. Calculated values of R_0, R_{ax} and R_{eq} distances (in Å) for the STH in AgCl compared with those derived for the $AgCl_6^{4-}$ complex formed in Ag^{2+}-doped NaCl and KCl host lattices[53]. The energy values (in eV) of the three crystal field transitions $b_{1g}(x^2-y^2) \rightarrow a_{1g}(3z^2-r^2)$, $b_{1g}(x^2-y^2) \rightarrow b_{2g}(xy)$ and $b_{1g}(x^2-y^2) \rightarrow e_g(xz,yz)$ measured for KCl:Ag^{2+} [36] are also shown and compared to the transition at 1.2 eV observed for the STH in AgCl. In accord with the analysis given in this work such a transition is assigned as $b_{1g}(x^2-y^2) \rightarrow a_{1g}(3z^2-r^2)$.

System	R_0(Å)	R_{ax}	R_{eq}	$R_{ax}- R_{eq}=3\varepsilon$	$a_{1g}(3z^2-r^2)$	$b_{2g}(xy)$	$e_g(xz,yz)$
KCl: Ag^{2+}	2.66	3.0	2.55	0.45	~1.55	1.97	2.21
NaCl: Ag^{2+}	2.63	2.84	2.56	0.28			
AgCl: Ag^{2+}	2.61	2.85	2.49	0.36	1.2		

Figure captions

Figure 1. . Illustration of the various quantities involved in the simple model. On the top we represent the geometry of the system for the centers q_1 and q_2 along the migration coordinate, starting when the distortion is localized on the first complex (left), finishing when it is localized on the second complex (right) and being perfectly delocalized between both situations (middle). In the middle and lower insets we represent the energy surface, orbital energies and character of the orbitals for the low and high-covalency limits, respectively.

Figure 2. (a) The small cell bounded by the blue lines was used for the band-structure calculations and the $3 \times 3 \times 3$ supercell (large cell) was used for the polaronic-transport calculations with the initially distorted $\mathrm{AgCl_6}$ complex indicated by the red Ag^{2+} ion. Ag^{+} ions are shown in gray and Cl^{-} ions are shown in green. (b) The STH in the AgCl lattice. X, Y and Z are the Ag ions closest to the $\mathrm{Ag^{2+}}$ ion and the circles indicate $\mathrm{Cl^{-}}$ ions. (c) The two kinds of Jahn–Teller distortions, compression (left) and elongation (right) which break the $\mathrm{O_h}$ space-group symmetry (middle).

Figure 3. (a) Calculated band structure of AgCl using PBEsol and U values $U_{\mathrm{Ag(s)}} = 4.0\ \mathrm{eV}$ and $U_{\mathrm{Cl(p)}} = 5.0\ \mathrm{eV}$. (b) Calculated band structure of AgBr using PBEsol and U values $U_{\mathrm{Ag(s)}} = 5.25\ \mathrm{eV}$ and $U_{\mathrm{Br(p)}} = 3.0\ \mathrm{eV}$. (c) Dependence of direct and indirect bandgaps of AgCl upon $U_{\mathrm{Ag(s)}}$ value fixing $U_{\mathrm{Cl(p)}} = 5.0\ \mathrm{eV}$. (d) Dependence of direct and indirect bandgaps of AgCl upon $U_{\mathrm{Cl(p)}}$ value fixing $U_{\mathrm{Ag(s)}} = 4.0\ \mathrm{eV}$. (e) Dependence of direct and indirect bandgaps of AgBr upon $U_{\mathrm{Ag(s)}}$ value fixing $U_{\mathrm{Br(p)}} = 3.0\ \mathrm{eV}$. (f) Dependence of direct and indirect bandgaps of AgBr upon $U_{\mathrm{Br(p)}}$ value fixing $U_{\mathrm{Ag(s)}} = 5.25\ \mathrm{eV}$.

Figure 4. Activation barriers for polaronic hopping in AgCl for the 8 inequivalent paths, (a)-(h) with initial (left) and final (right) structures shown in each plot. The hop lengths are also indicated with $R_{\mathrm{L}} = 2.75\ \mathrm{Å}$. The distortions of the hole-hosting $\mathrm{AgCl_6}$ complex (red) are shown with a 25 % enhancement for the sake of clarity.

Figure 5. Sketch of the bonding between two Ag $4d_{x2-y-2}$ orbitals through the 3p orbitals of the Cl ligands in the Y (left) and XY (right) configurations.

Figure 1

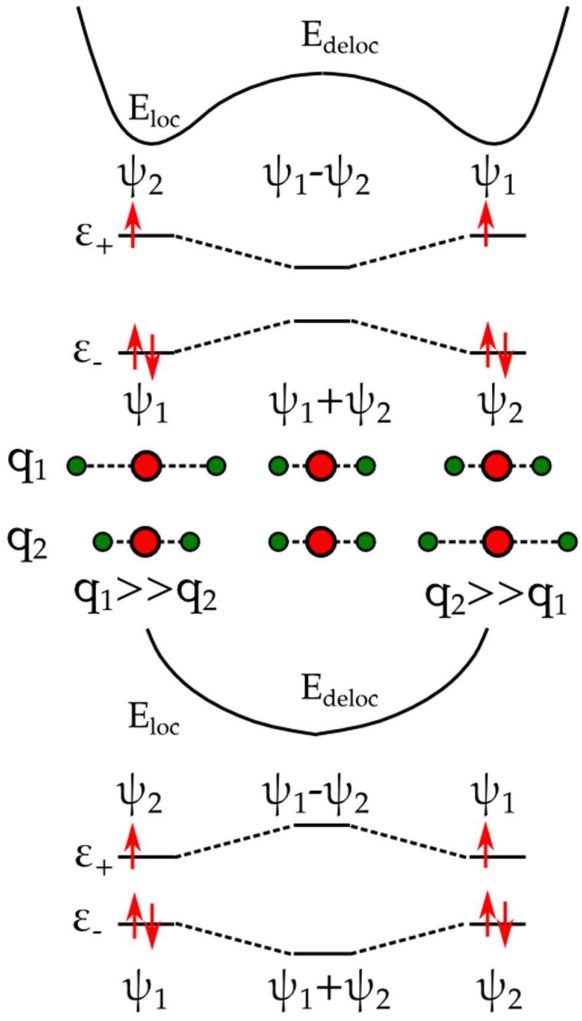
E_deloc
E_loc
ψ2
ψ1-ψ2
ψ1
ε+
ε-
ψ1
ψ1+ψ2
ψ2
q1
q2
q1>>q2
q2>>q1
E_deloc
E_loc
ψ2
ψ1-ψ2
ψ1
ε+
ε-
ψ1
ψ1+ψ2
ψ2

Figure 2

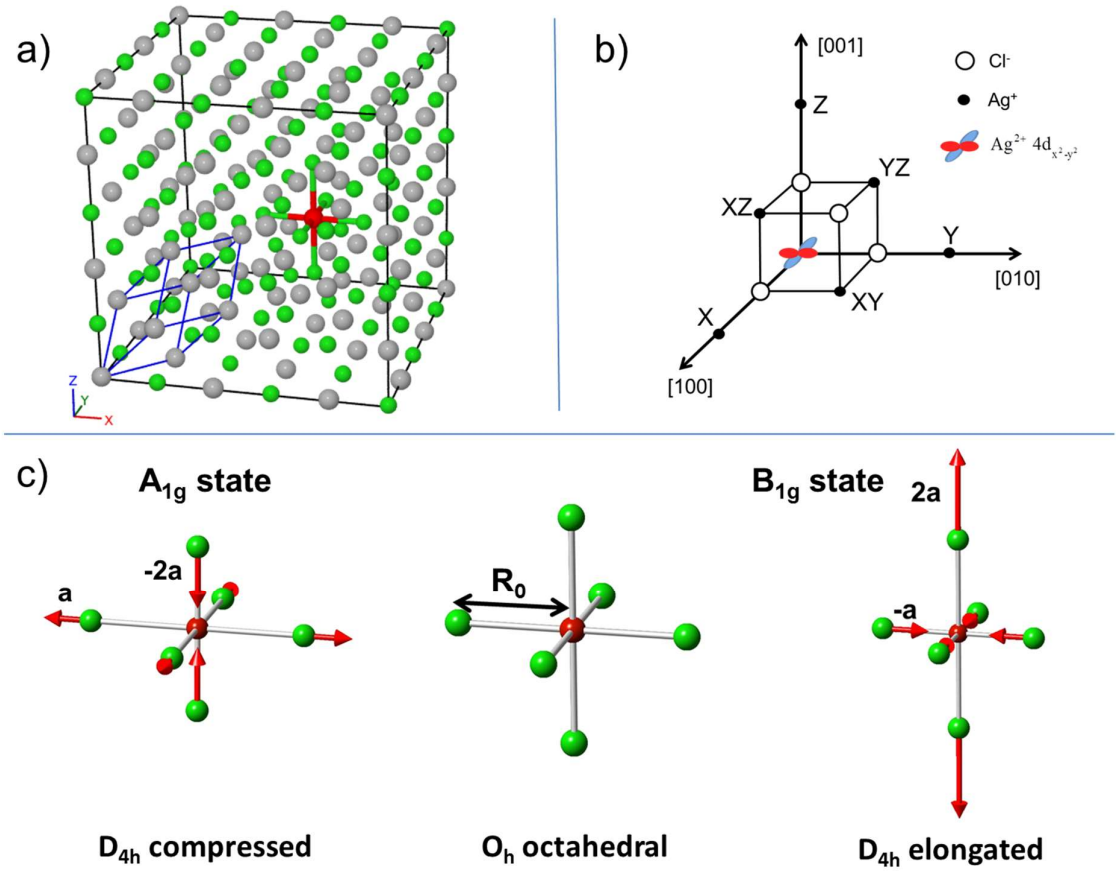
a)
b)
[001]
Z
Cl-
Ag+
Ag2+ 4dx2-y2
YZ
XZ
Y
[010]
XY
X
[100]
c)
A1g state
-2a
a
R0
B1g state
2a
-a
D4h compressed
Oh octahedral
D4h elongated

Figure 3

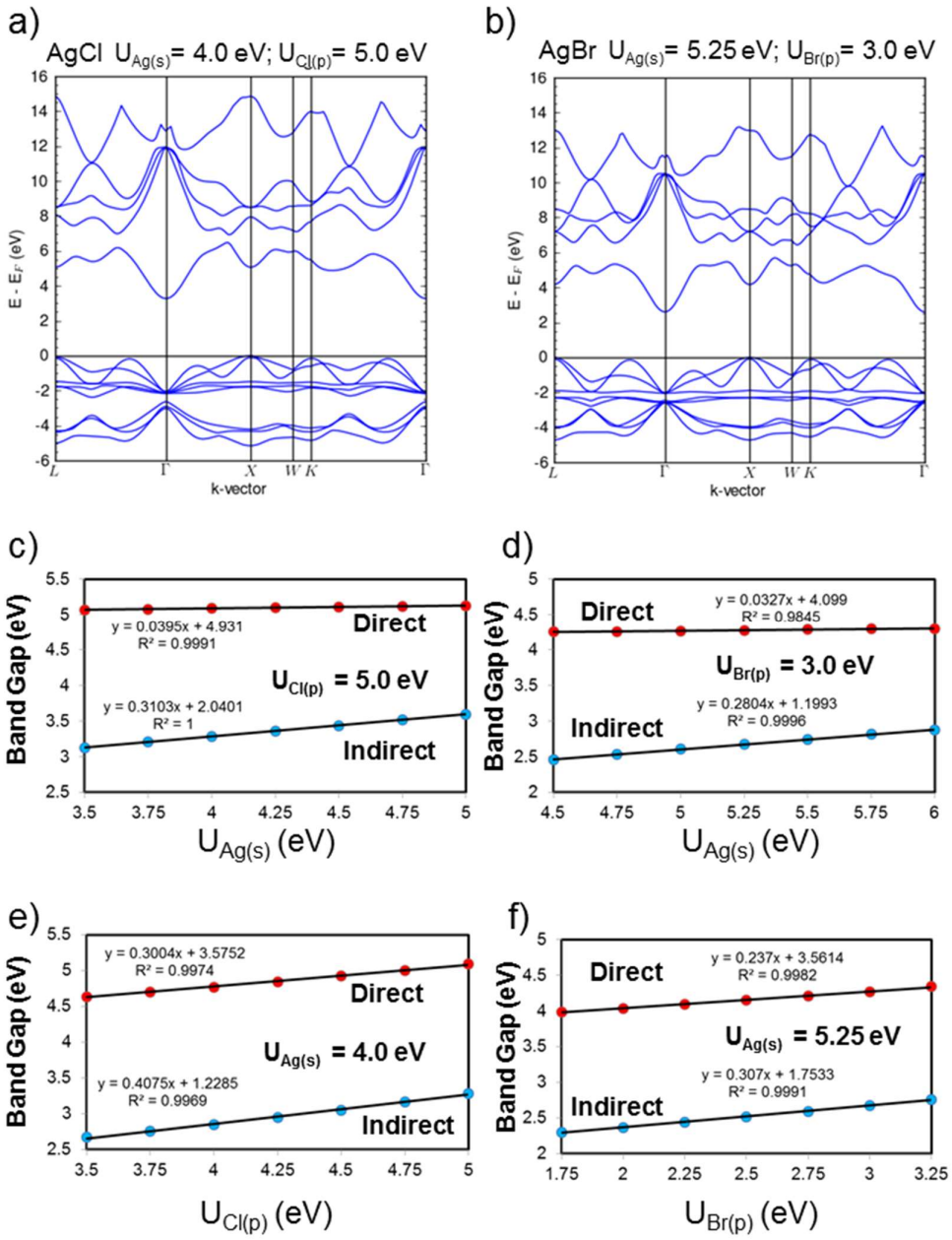
a)
AgCl $U_{Ag(s)}$= 4.0 eV; $U_{Cl(p)}$= 5.0 eV
E - E_F (eV)
k-vector
L Γ X W K Γ
b)
AgBr $U_{Ag(s)}$= 5.25 eV; $U_{Br(p)}$= 3.0 eV
E - E_F (eV)
k-vector
L Γ X W K Γ
c)
Band Gap (eV)
y = 0.0395x + 4.931
R² = 0.9991
Direct
$U_{Cl(p)}$ = 5.0 eV
y = 0.3103x + 2.0401
R² = 1
Indirect
$U_{Ag(s)}$ (eV)
d)
Band Gap (eV)
Direct
y = 0.0327x + 4.099
R² = 0.9845
$U_{Br(p)}$ = 3.0 eV
Indirect
y = 0.2804x + 1.1993
R² = 0.9996
$U_{Ag(s)}$ (eV)
e)
Band Gap (eV)
y = 0.3004x + 3.5752
R² = 0.9974
Direct
$U_{Ag(s)}$ = 4.0 eV
y = 0.4075x + 1.2285
R² = 0.9969
Indirect
$U_{Cl(p)}$ (eV)
f)
Band Gap (eV)
Direct
y = 0.237x + 3.5614
R² = 0.9982
$U_{Ag(s)}$ = 5.25 eV
Indirect
y = 0.307x + 1.7533
R² = 0.9991
$U_{Br(p)}$ (eV)

Figure 4

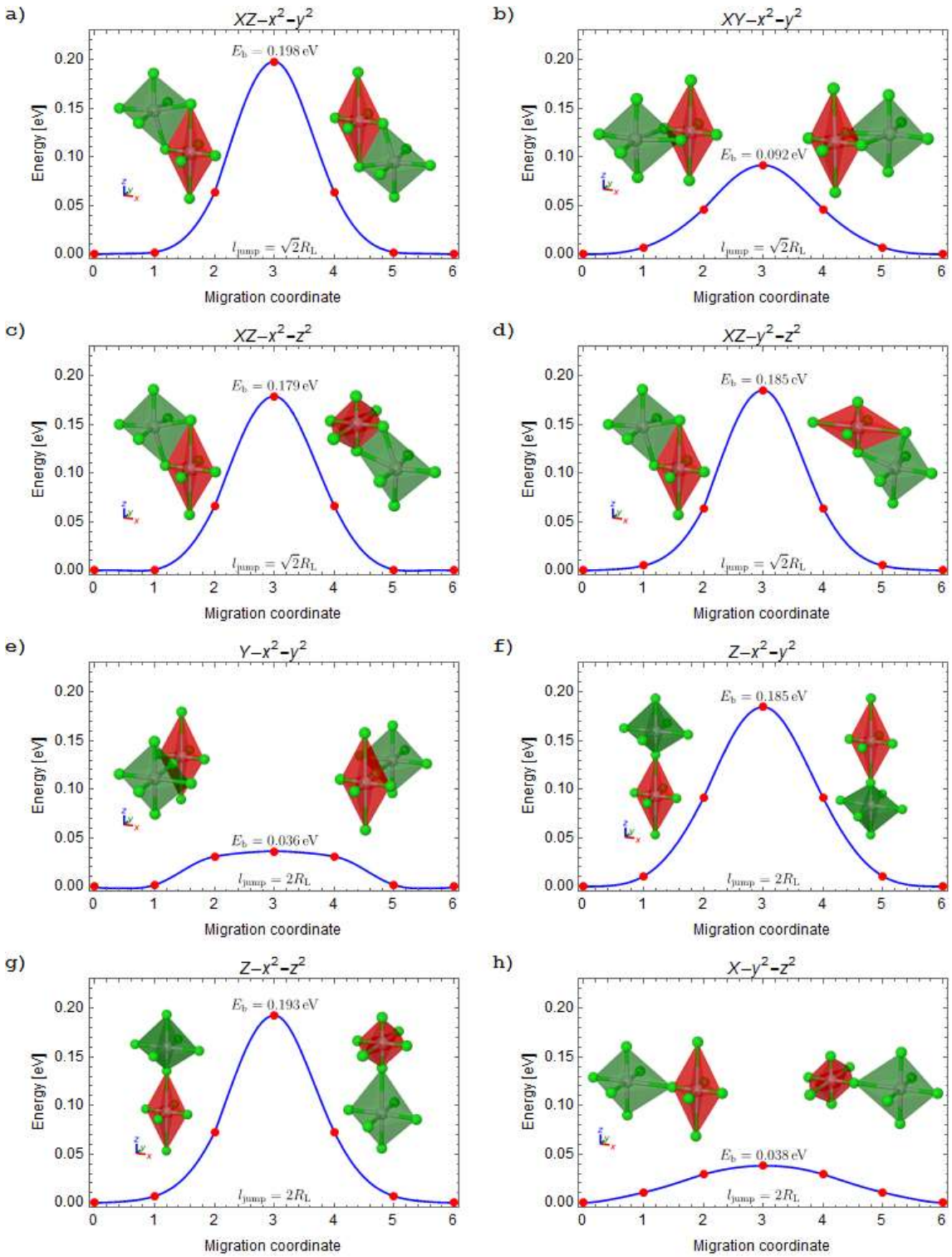
a)
XZ–x²–y²
E_b = 0.198 eV
l_jump = √2 R_L
b)
XY–x²–y²
E_b = 0.092 eV
l_jump = √2 R_L
c)
XZ–x²–z²
E_b = 0.179 eV
l_jump = √2 R_L
d)
XZ–y²–z²
E_b = 0.185 eV
l_jump = √2 R_L
e)
Y–x²–y²
E_b = 0.036 eV
l_jump = 2 R_L
f)
Z–x²–y²
E_b = 0.185 eV
l_jump = 2 R_L
g)
Z–x²–z²
E_b = 0.193 eV
l_jump = 2 R_L
h)
X–y²–z²
E_b = 0.038 eV
l_jump = 2 R_L
Energy [eV]
Migration coordinate

Figure 5.

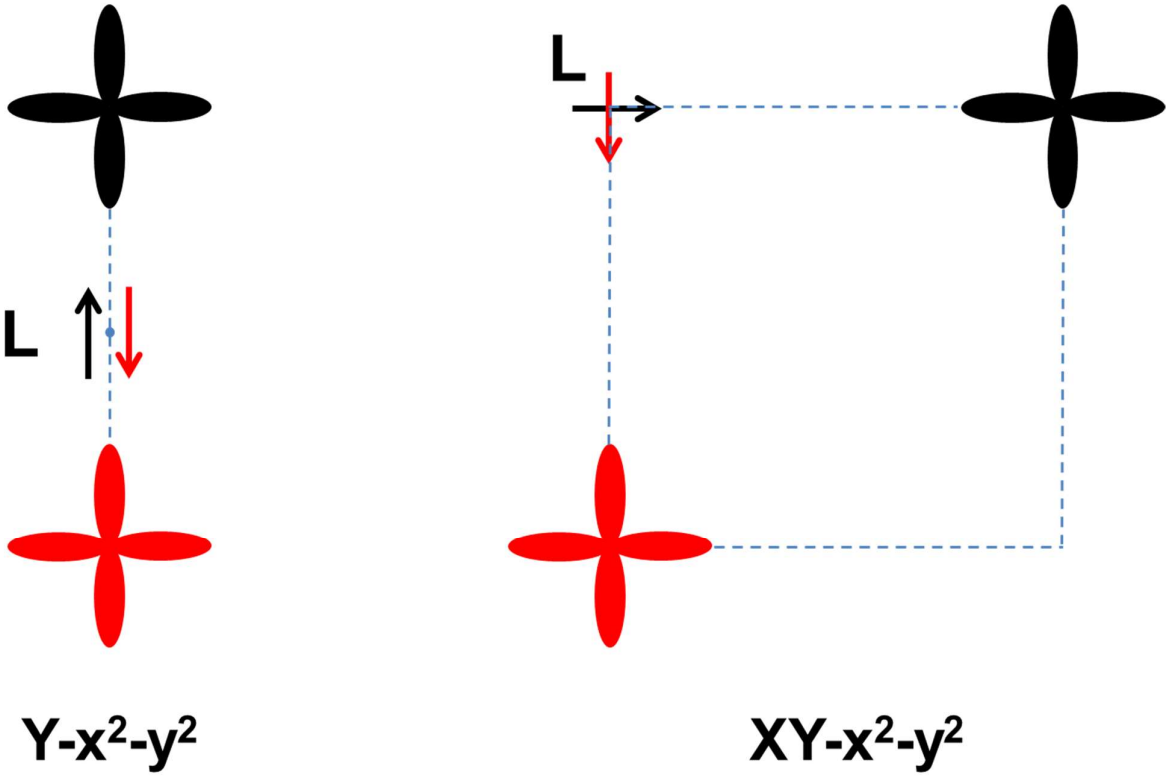

GRAPHICAL TABLE OF CONTENTS